iScience

CellPress
OPEN ACCESS

Article

Insulin receptor isoform B is required for efficient proinsulin processing in pancreatic β cells

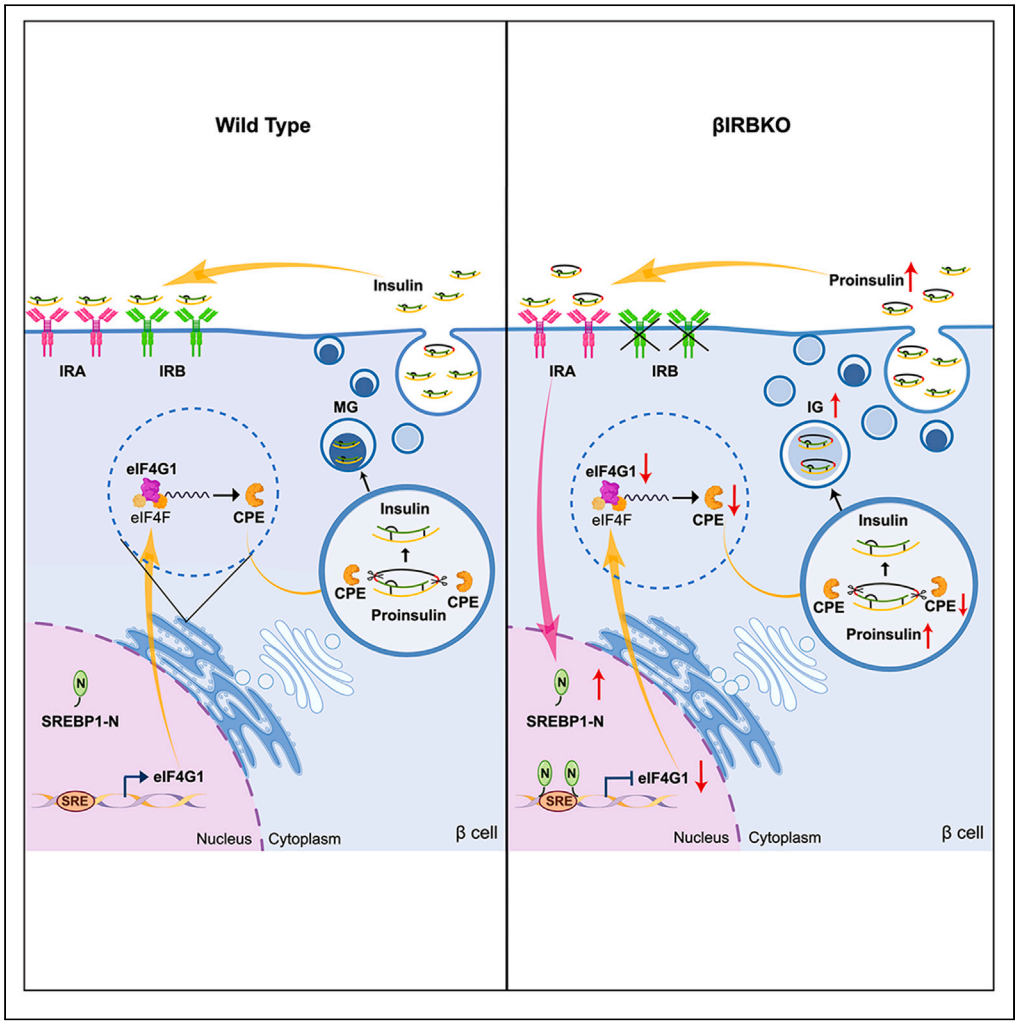

Mingchao Jiang, Ning Wang, Yuqin Zhang, ..., Bin Liang, Weiping Zhang, Yingjie Wu

liangb73@ynu.edu.cn (B.L.)
zbtb20@aliyun.com (W.Z.)
yingjiewu@dmu.edu.cn (Y.W.)

Highlights

β cell IRB deficiency impairs proinsulin processing under high-fat stress

IRB KO in β cells up-regulated SREBP1 to inhibit eIF4G1 and induce lipotoxicity

Specific SREBP1 inhibitor, fatostatin, rescued IRB KO phenotypes

Autocrine proinsulin forms a feedback loop through IRA and ERK in βIRBKO mice

Jiang et al., iScience *27*, 110017
July 19, 2024
https://doi.org/10.1016/j.isci.2024.110017

iScience

CellPress
OPEN ACCESS

Article

Insulin receptor isoform B is required for efficient proinsulin processing in pancreatic β cells

Mingchao Jiang,[1,7] Ning Wang,[1,7] Yuqin Zhang,[1] Jinjin Zhang,[2] Youwei Li,[1,3] Xiu Yan,[1] Honghao Zhang,[1] Chengbin Li,[4] Youfei Guan,[5] Bin Liang,[4,*] Weiping Zhang,[6,*] and Yingjie Wu[1,2,8,*]

SUMMARY

The insulin receptor (INSR, IR) has two isoforms, IRA and IRB, through alternative splicing. However, their distinct functions *in vivo* remain unclear. Here we generated β cell-specific IRB knockout (KO) mice (βIRBKO). The KO mice displayed worsened hyperinsulinemia and hyperproinsulinemia in diet-induced obesity due to impaired proinsulin processing in β cells. Mechanistically, loss of IRB suppresses eukaryotic translation initiation factor 4G1 (eIF4G1) by stabilizing the transcriptional receptor sterol-regulatory element binding protein 1 (SREBP1). Moreover, excessive autocrine proinsulin in βIRBKO mice enhances the activity of extracellular signal-regulated kinase (ERK) through the remaining IRA to further stabilize nuclear SREBP1, forming a feedback loop. Collectively, our study paves the way to dissecting the isoform-specific function of IR *in vivo* and highlights the important roles of IRB in insulin processing and protecting β cells from lipotoxicity in obesity.

INTRODUCTION

Alternative splicing (AS) allows the production of functionally distinct protein isoforms from a single gene.[1] This is a prevalent post-transcriptional regulatory machinery as human genes undergo AS in 92–94% of cases.[2] In mammalian evolution, AS is often cited as one of the major drivers of phenotypic complexity.[3] AS dysregulation contributes to disease development and susceptibility.[4] IR (insulin receptor, INSR) undergoes AS to produce two distinct mRNA isoforms, generating two structurally and functionally distinct insulin receptors, IRA and IRB.[5] IRA lacks exon 11, which contains 36 base pairs encoding 12 amino acids, while IRB is the product of the exon inclusion event.[6] IRA acts as a receptor for insulin, proinsulin, and insulin-like growth factor 2 (IGF2), mediating proliferative effects in embryonic and tumor tissues, while IRB is more specialized to insulin action in metabolic tissues of, such as the liver, muscle, and fat.[7–9] The ratio of IRA to IRB is dynamic but strictly regulated in different organs and tissues. Given the central role of IR in insulin signaling and the development of insulin resistance, it remains a fundamental question in the metabolism field regarding the isoform-specific functions of IRA and IRB.

As the producer of insulin, β cells also express abundant IR to respond to insulin signaling. Kulkarni et al. used RIP-Cre to knock out both IR isoforms in pancreatic β cells and found that mice exhibited reduced insulin secretion in the first phase after glucose stimulation and showed progressive glucose intolerance.[10] This knockout (KO) model was later shown to develop impaired proinsulin processing and insulin resistance-induced loss of compensatory proliferation.[11,12] However, these studies have suffered from a paucity of functional distinctions between IRA and IRB isoforms. Leibiger et al. used transient overexpression *in vitro* models and revealed the selective insulin signaling of IRA and IRB.[13] Subsequently, Nevado et al. generated cells only expressing the IRA but not the IRB isoform using IR-knockout immortalized neonatal hepatocytes and found that the IRA isoform acts on glucose uptake of hepatocytes via GLUT-related cotransporter.[14] Escribano et al. also revealed in immortalized mouse β cell lines that IR-deficient β cells exclusively expressing IRA were more sensitive to insulin and insulin-like growth factor 1 (IGF-I)-induced proliferation than those expressing IRB.[15] To date, studies to distinguish the function of these two isoforms have been cell line based. Therefore, the pathophysiological roles of IR isoforms remain unclear. This gap in knowledge is because of the technical challenge in targeting the small exon 11 of the *IR* gene, particularly in a conditional manner.

[1]Institute for Genome Engineered Animal Models of Human Diseases, National Center of Genetically Engineered Animal Models for International Research, Liaoning Provence Key Lab of Genome Engineered Animal Models, Dalian Medical University, Dalian, Liaoning 116000, China
[2]Shandong Provincial Hospital, School of Laboratory Animal & Shandong Laboratory Animal Center, Science and Technology Innovation Center, Shandong First Medical University & Shandong Academy of Medical Sciences, Jinan, Shandong 250021, China
[3]Haidu College, Qingdao Agricultural University, Laiyang, Shandong 265200, China
[4]Center for Life Sciences, School of Life Sciences, Yunnan University, Kunming, Yunnan 650091, China
[5]Advanced Institute for Medical Sciences, Dalian Medical University, Dalian 116044, China
[6]Department of Pathophysiology, Naval Medical University, Shanghai 200433, China
[7]These authors contributed equally
[8]Lead contact
*Correspondence: liangb73@ynu.edu.cn (B.L.), zbtb20@aliyun.com (W.Z.), yingjiewu@dmu.edu.cn (Y.W.)
https://doi.org/10.1016/j.isci.2024.110017

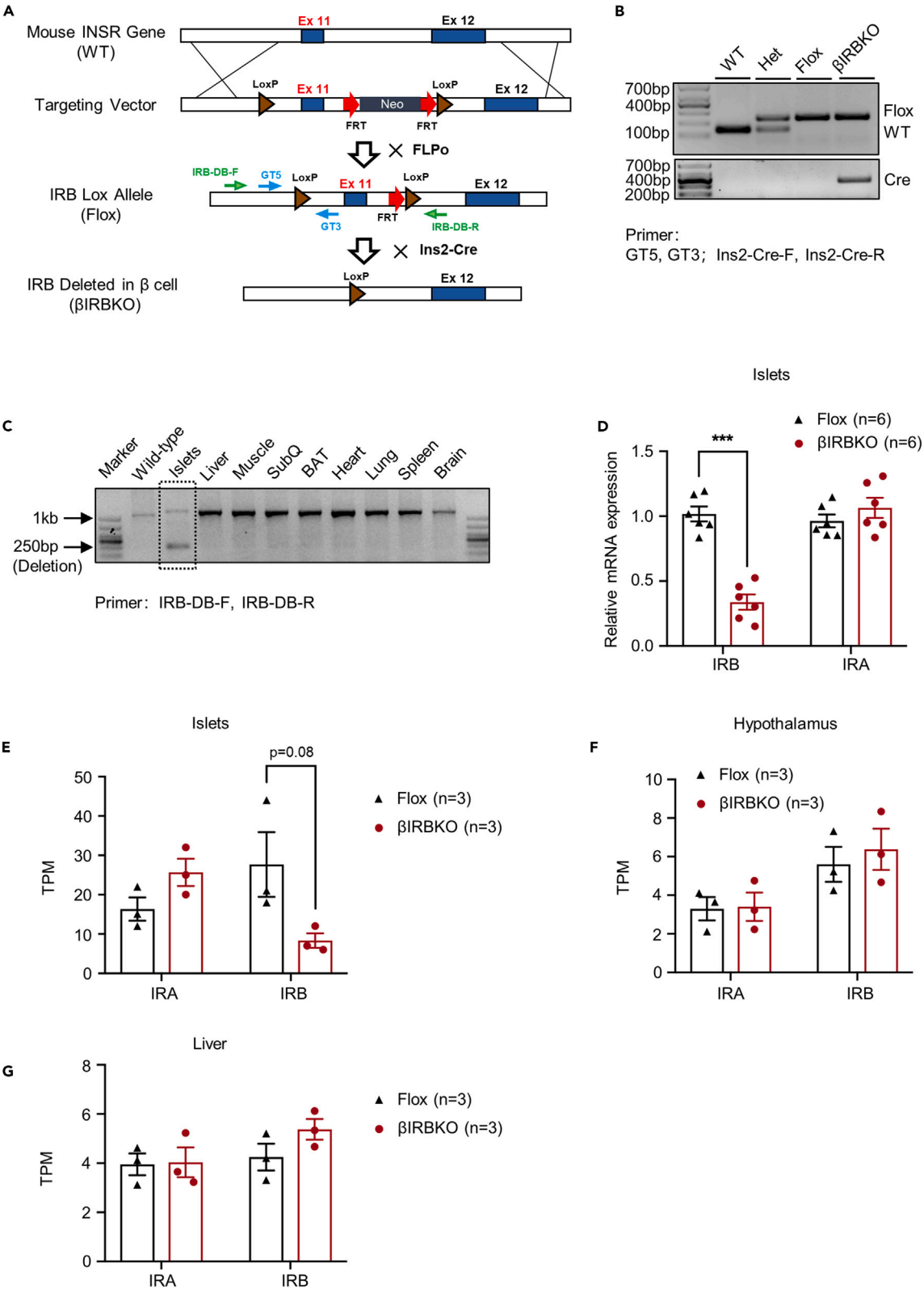
A
Mouse INSR Gene (WT)
Ex 11
Ex 12
Targeting Vector
LoxP
Ex 11
Neo
LoxP
Ex 12
FRT
FRT
FLPo
IRB Lox Allele (Flox)
IRB-DB-F
GT5
LoxP
Ex 11
LoxP
Ex 12
GT3
FRT
IRB-DB-R
Ins2-Cre
IRB Deleted in β cell (βIRBKO)
LoxP
Ex 12
B
WT
Het
Flox
βIRBKO
700bp
400bp
100bp
Flox
WT
700bp
400bp
200bp
Cre
Primer:
GT5, GT3; Ins2-Cre-F, Ins2-Cre-R
C
Marker
Wild-type
Islets
Liver
Muscle
SubQ
BAT
Heart
Lung
Spleen
Brain
1kb
250bp
(Deletion)
Primer: IRB-DB-F, IRB-DB-R
D
Islets
Flox (n=6)
βIRBKO (n=6)
***
Relative mRNA expression
1.5
1.0
0.5
0.0
IRB
IRA
E
Islets
p=0.08
Flox (n=3)
βIRBKO (n=3)
TPM
50
40
30
20
10
0
IRA
IRB
F
Hypothalamus
Flox (n=3)
βIRBKO (n=3)
TPM
10
8
6
4
2
0
IRA
IRB
G
Liver
Flox (n=3)
βIRBKO (n=3)
TPM
8
6
4
2
0
IRA
IRB

Figure 1. Generation of β cell-specific IRB knockout mice

(A) Schematic diagram of βIRBKO mice construction. Arrows indicate the primer sets used for PCR genotyping.

(B) PCR genotyping of Flox and βIRBKO mice with primer set GT5 and GT3 shown in (A). Bottom panel is the PCR result for *Cre* marker.

(C) PCR genotyping in various tissues using primer set IRB-DB-F and IRB-DB-R shown in (A). Note that a smaller deletion band due to Cre excision was detected only in islets of βIRBKO mice.

(D) Real-time PCR analysis of *IRA* and *IRB* expression from isolated islets ($n = 6$ animals).

(E–G) Expression of *IRA* and *IRB* in TPM in islets (E)($p = 0.08$), hypothalamus (F) and liver (G) of Flox and βIRBKO mice ($n = 3$ animals). TPM, Transcripts Per Kilobase of exon model per Million mapped reads. All data presented are from male mice. Data are presented as mean ± SEM. Statistical analysis is performed using a Student's t test and statistical significance is shown as $^{***}p < 0.001$.

To overcome this long-lasting challenge, we delved into constructing a unique mouse model of specific knockout of IRB in pancreatic β cells (βIRBKO). By investigating its metabolic phenotype in both basal and high-fat diet (HFD) challenge conditions, we reported hyperinsulinemia and hyperproinsulinemia caused by IRB deficiency due to proinsulin processing. The IRB-deficient β cells undergo lipotoxicity due to dysregulated SREBP1, which leads to downregulation of eIF4G1 and, consequently, the translation of carboxypeptidases E (CPE), the key enzyme for proinsulin hydrolysis. Our work hereby provides *in vivo* evidence of IRB's essential role in efficient insulin processing and secretion in response to insulin signaling.

RESULTS

Generation of β cell-specific IRB knockout mice

The difference between the two IR isoforms is that IRB retains exon 11, whereas IRA skips it. We managed to insert Flox sites on both ends of exon 11 without interfering with its splicing, resulting in the specific targeting of IRB. We then bred IRB floxed mice with Ins2-Cre mice to construct a βIRBKO mouse model (Figures 1A and 1B). It is worth noting that the RIP-Cre line commonly used in targeting β cells is based on the short rat *Ins2* promoter fragment and shows recombination activity in hypothalamic neurons, creating caveats in interpreting metabolic phenotype from a β cell-specific perspective.[16] To overcome this off-target issue, we employed the Ins2-Cre knock-in mouse line, which showed no Cre activity in the mouse hypothalamic neurons.[17]

PCR genotyping confirmed that the *LoxP* site is only present in the Floxed mice (Figure 1B). With Cre expression, deletion of exon 11 is detected only in pancreatic islets but not in the liver, muscle, subcutaneous fat, brown adipose tissue (BAT), heart, lung, spleen, and especially brain, confirming the tissue specificity of Cre expression (Figure 1C). Consistently, *IRB* mRNA level is specifically reduced in the islets of the βIRBKO mice, though not completely, as islets contain other cell types as well (Figure 1D).[18] Through 3rd generation sequencing, we confirmed that the expression of *IRB* was greatly reduced in the islets of βIRBKO mice, while the hypothalamus and liver were not affected (Figures 1E–1G). Therefore, by successfully constructing this unique βIRBKO mouse model, we are confident that the metabolic phenotype, if any, should be restricted to β cell IRB deficiency instead of the confounding off-target effects in the hypothalamus.

βIRBKO mice worsen hyperproinsulinemia, insulin resistance, and glucose intolerance in diet-induced obesity

HFD mice and *db/db* mice are two widely used mouse insulin resistance models exhibiting hyperproinsulinemia.[19] We then examined the expression of the two isoforms of IR in the islets of these two classic models. The expression of IRB in islets was significantly reduced, while the expression of IRA was inversely increased in wild-type (WT) mice fed HFD for 24 weeks compared with mice fed regular chow (RC) (Figure 2A). 16-week-old *db/db* mice showed the same IR isoform pattern compared to control *db/m* mice (Figure 2B). These results suggest a possible pathogenic role of IR isoform switching in the progression of insulin resistance and diabetes.

On RC feeding, βIRBKO mice exhibited normal metabolic phenotype in regards of body weight, organ sizes, glucose tolerance, and insulin sensitivity (Figures 2C, 2D, S1A, and S1B). Over a course of 24-week HFD feeding, the KO mice still showed the same weight gain as the control mice, supported by their same organ sizes (Figure 2D). However, despite the blunted phenotype in body weight, obese βIRBKO mice developed worse glucose intolerance and were less sensitive to exogenous insulin stimulation compared with the Flox control mice (Figures 2E and 2F). In line with their insulin resistance phenotype, an inhibition of AKT phosphorylation was detected in the KO livers (Figures 2G and 2H). Consistently, obese βIRBKO mice exhibited higher fasting plasma proinsulin and insulin levels, and the plasma proinsulin to insulin (P/I) ratio was also noticeably altered compared to Flox mice (Figures 2I–2K). Hyperproinsulinemia is a highly specific marker for insulin resistance.[20] In addition to being strongly associated with type 2 diabetes development, elevated P/I ratio also increases the risk of hypertension and cardiovascular disease.[21–23] These data suggest that loss of IRB causes β cells to release more proinsulin into the blood under high-fat exposure without interfering with body weight, causing hyperinsulinemia and hyperproinsulinemia, which aggravate insulin resistance and glucose intolerance.

β cell IRB deficiency increases proinsulin content in islets

To investigate whether IRB deficiency causes abnormal secretion of insulin and proinsulin in β cells, we examined circulating insulin and proinsulin levels within 2 h of glucose-stimulated insulin secretion (GSIS) assay. Upon glucose challenge, serum proinsulin levels were consistently significantly higher in the KO group than in the control group, both in the first and second secretion phases, and the total amount of secretion was also significantly increased (Figure 3A). Although the insulin secretion curve of βIRBKO mice after glucose stimulation was above that of Flox mice (Figure 3B), the P/I ratio was still higher in the knockout group (Figure 3C), suggesting an increase in both absolute and relative

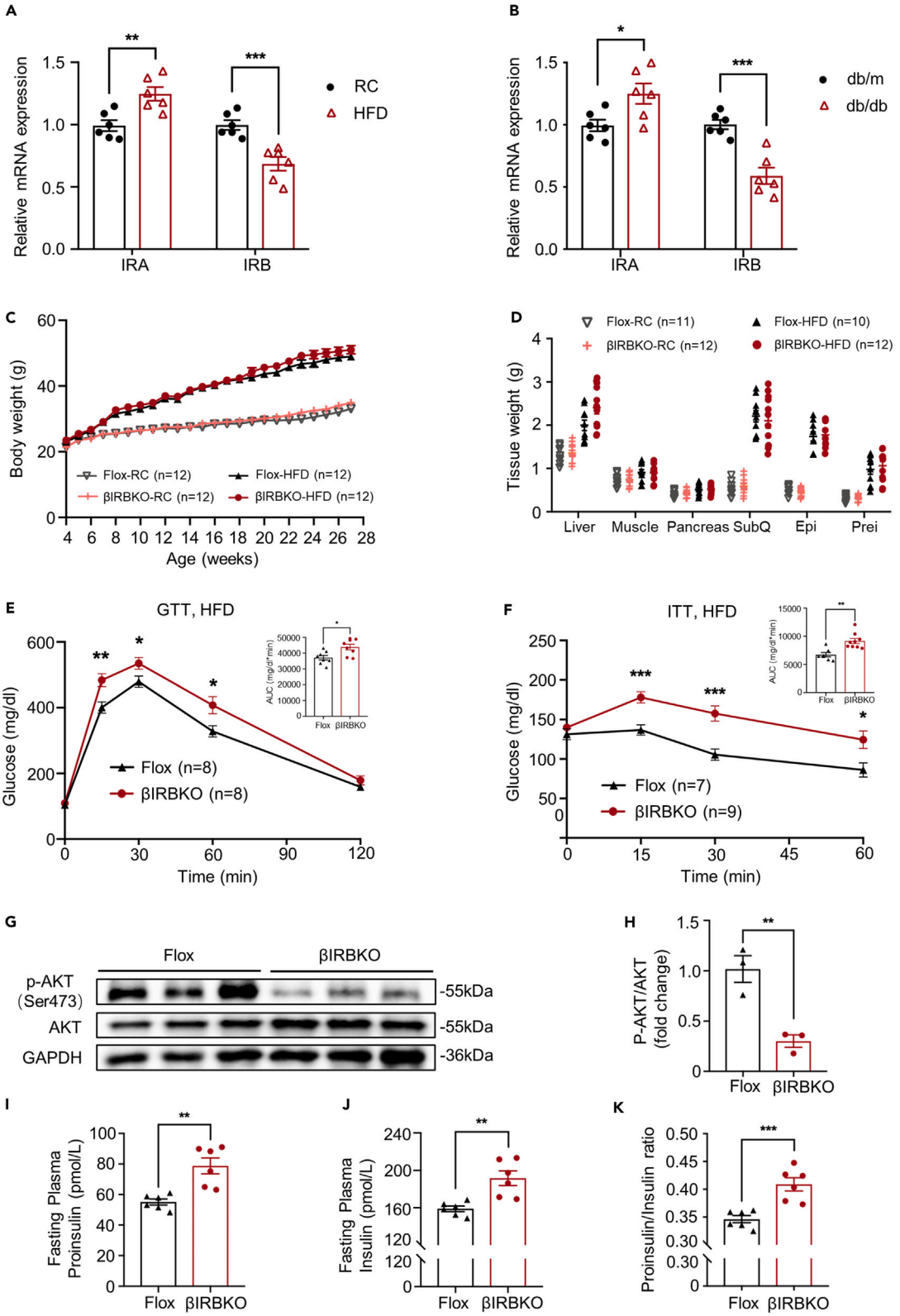
A
Relative mRNA expression
RC
HFD
IRA
IRB
B
db/m
db/db
C
Body weight (g)
Flox-RC (n=12)
Flox-HFD (n=12)
βIRBKO-RC (n=12)
βIRBKO-HFD (n=12)
Age (weeks)
D
Flox-RC (n=11)
Flox-HFD (n=10)
βIRBKO-RC (n=12)
βIRBKO-HFD (n=12)
Tissue weight (g)
Liver
Muscle
Pancreas
SubQ
Epi
Prei
E
GTT, HFD
Glucose (mg/dl)
Flox (n=8)
βIRBKO (n=8)
Time (min)
AUC (mg/dl*min)
F
ITT, HFD
Glucose (mg/dl)
Flox (n=7)
βIRBKO (n=9)
Time (min)
G
Flox
βIRBKO
p-AKT (Ser473)
AKT
GAPDH
-55kDa
-55kDa
-36kDa
H
P-AKT/AKT (fold change)
I
Fasting Plasma Proinsulin (pmol/L)
J
Fasting Plasma Insulin (pmol/L)
K
Proinsulin/Insulin ratio

Figure 2. βIRBKO mice develop hyperproinsulinemia, insulin resistance, and glucose intolerance

(A) Real-time PCR analysis of *IRA* and *IRB* expression from isolated islets of WT mice after 24 weeks of HFD or RC (n = 6 animals).

(B) Real-time PCR analysis of *IRA* and *IRB* expression from isolated islets of 16-week-old db/db and db/m mice (n = 6 animals).

(C) Body weight of male Flox and βIRBKO mice fed on RC or HFD from 4 weeks to 28 weeks (n = 12 animals).

(D) Tissue mass of male Flox and βIRBKO mice (n = 10–12 animals).

(E and F) Glucose tolerance test (E) and insulin tolerance test (F) of Flox and βIRBKO mice after 24 weeks of HFD (n = 7–9 animals). The area under curves are shown as insets.

(G) *p*-AKT (Ser473) and total AKT levels in liver of Flox or βIRBKO mice.

(H) Relative phosphorylation level of AKT quantified from (G).

(I–K) Fasting plasma proinsulin levels (I), insulin levels (J) and proinsulin/insulin ratio (K) measured with ELISA in Flox or βIRBKO mice (n = 6 animals). All data were collected with male mice after 24 weeks of HFD if not stated otherwise. Data are presented as mean ± SEM. Statistical analysis is performed using a Student's t test and statistical significance is shown as $*p < 0.05$, $**p < 0.01$, and $***p < 0.001$.

proinsulin secretion in βIRBKO mice. However, there were no significant differences in serum insulin and proinsulin levels between βIRBKO mice and Flox mice fed with RC (Figures S2A and S2B).

To explore whether the aforementioned changes are due to abnormal hypersecretion or enhanced proinsulin production, we isolated islets from both mouse groups and stimulated them with different concentrations of glucose *in vitro*. The intracellular proinsulin content detected after ultrasound fragmentation was increased by the loss of IRB, and so was the proinsulin to insulin ratio, regardless in a low-glucose environment or stimulated by high-glucose at 16.8 mM (Figures 3D–3F). In addition, the protein levels of glucokinase (GCK) and glucose transporter 2 (GLUT2) in βIRBKO islets were not significantly changed compared with Flox mice regardless of insulin stimulation (Figure S2C). GCK and GLUT2 control the initiation of insulin secretion. Our data indicate that insulin secretion in IRB-deficient β cells is not hyperactive. IHC staining of pancreatic sections revealed higher proinsulin content in the βIRBKO islets (Figures 3G, 3H, and S3A), consistent with the *in vivo* and *in vitro* GSIS. In addition, increased *Insulin 1* (*Ins1*) mRNA was detected in the isolated islets of βIRBKO mice (Figure 3I), and insulin levels in islets were also significantly increased (Figures S3B and S3C), suggesting that more insulin and proinsulin is produced in βIRBKO mice.

β cell IRB loss impairs the maturation of insulin secretion granules

The biosynthesis and maturation of insulin undergo a complex and dynamic process. Pre-proinsulin is translated at the ribosome of the rough endoplasmic reticulum (ER) after undergoing gene transcription and subsequently converted into proinsulin by signal peptidases after translocating into the lumen of the ER, which is then folded and forms disulfide bonds. Afterward, proinsulin is sorted and assembled into immature nascent granules in the Golgi apparatus.[24,25] A higher P/I ratio could result from the defects during this process. To ultimately detect any defect in insulin processing, we employed the ultrathin transmission electron microscopy (TEM) to examine sections of isolated islets from βIRBKO and Flox mice. TEM images showed that β cells from both groups were filled with vesicles. However, the IRB-deficient β cells contained a large number of newly synthesized proinsulin-rich secretory granules (SGs) characterized by immature granules with a lighter inner color and narrower outer transparent rings (halo), whereas the control group was predominantly occupied by mature granules with dark dense cores and wide halos (Figure 4A).[26,27] Statistical analysis of lower magnification images following the method of previous studies[28,29] showed a significant increase in the density of SGs in β cells lacking IRB (Figure 4B), while the proportion of mature granules did not match the increased density, indicating impaired granule maturation (Figure 4C). These data suggest that the excessive accumulation of proinsulin in β cells of obese βIRBKO mice is due to a blockage of the proinsulin maturation process.

β cell IRB deletion downregulates eIF4G1 expression and prevents CPE's translation process

Next, we sought to understand the underlying mechanism of how IRB deficiency impairs proinsulin processing. Within the secretory granules, proinsulin is processed by prohormone convertase (PC1/3, PC2) and CPE into its biologically active mature form, in which insulin is stored and released upon stimulation.[30] Tight regulation of PC1/3, PC2, and CPE is required for the appropriate production of mature insulin by β cells. We then examined the gene expression of the three key hydrolases, *PC1*, *PC2*, and *CPE* in proinsulin processing in pancreatic islets by 3rd generation sequencing. Surprisingly, there were no significant changes in the transcript levels of all three genes in obese βIRBKO mice (Figures 5A–5C). The mRNA expression levels detected by qPCR confirmed the sequencing results (Figure 5D). In contrast, a steep decrease in CPE protein levels but not PC1/3 and PC2 was detected in the βIRBKO mice (Figures 5E and 5F). IHC staining with a CPE-specific antibody clearly showed a weaker staining signal in the islets of βIRBKO mice compared to Flox mice (Figures 5G, 5H, and S4A). These data suggest that decreased CPE protein expression likely accounts for the impaired proinsulin processing.

The decreased CPE protein but unchanged gene transcription implies regulation at the post-transcriptional level. Previous studies have proposed that global regulation of translation initiation by nutrition is achieved primarily through the function of factors such as eIF4F, eIF2α, and 4E-binding proteins (4EBP).[31] eIF4F is a heterotrimer complex composed of eIF4G, eIF4E, and eIF4A, which is necessary for cap-dependent translation.[32] Therefore, we examined the expression of eIF4F-related components and found no apparent down-regulation of other factors except for the scaffolding protein eIF4G1 at the mRNA level (Figure 5I). Consistently, the eIF4G1 protein level was largely reduced in isolated islets from βIRBKO mice (Figures 5J and 5K). In contrast, transcription of *eIF4E* was enhanced (Figure 5I), which may be a compensational effect to the reduction of eIF4G1. In addition, there was no significant change in the protein

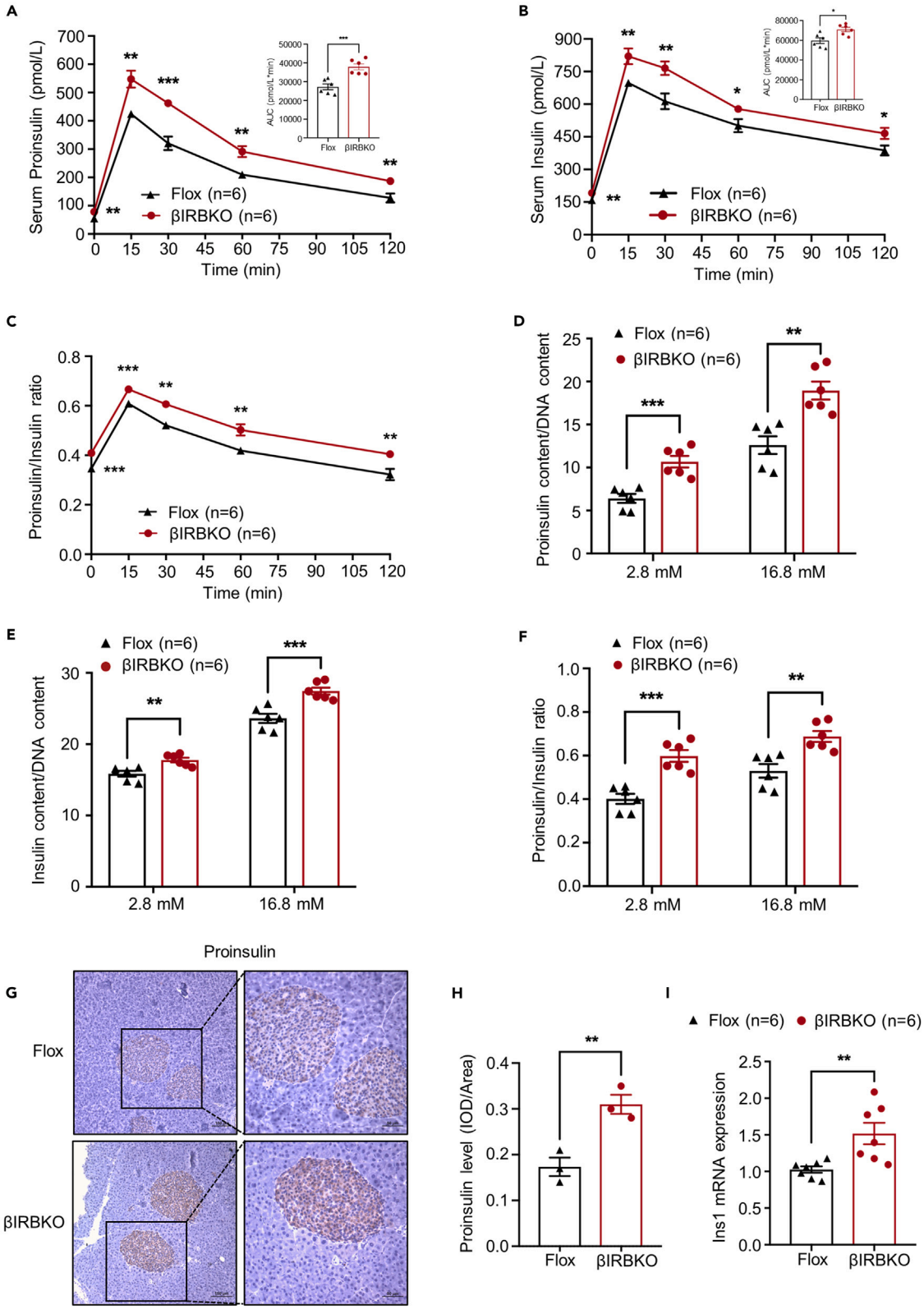
A
Serum Proinsulin (pmol/L)
Time (min)
Flox (n=6)
βIRBKO (n=6)
AUC (pmol/L*min)
Flox
βIRBKO
B
Serum Insulin (pmol/L)
Time (min)
Flox (n=6)
βIRBKO (n=6)
AUC (pmol/L*min)
Flox
βIRBKO
C
Proinsulin/Insulin ratio
Time (min)
Flox (n=6)
βIRBKO (n=6)
D
Proinsulin content/DNA content
Flox (n=6)
βIRBKO (n=6)
2.8 mM
16.8 mM
E
Insulin content/DNA content
Flox (n=6)
βIRBKO (n=6)
2.8 mM
16.8 mM
F
Proinsulin/Insulin ratio
Flox (n=6)
βIRBKO (n=6)
2.8 mM
16.8 mM
Proinsulin
G
Flox
βIRBKO
H
Proinsulin level (IOD/Area)
Flox
βIRBKO
I
Flox (n=6)
βIRBKO (n=6)
Ins1 mRNA expression
Flox
βIRBKO

Figure 3. βIRBKO mice exhibit elevated proinsulin secretion level and proinsulin content

(A–C) Glucose stimulated proinsulin secretion level (A), insulin secretion level (B) and proinsulin/insulin ratio (C) measured with ELISA in blood serum of Flox and βIRBKO mice (n = 6 animals). The area under curves are shown in the inset.

(D–F) Proinsulin content (D), insulin content (E), and proinsulin/insulin ratio (F) measured with ELISA in isolated islets stimulated with 2.8mM or 16.8mM glucose for 1 h of Flox and βIRBKO mice (n = 6 animals), normalized to DNA content in islets.

(G) Representative IHC staining images for proinsulin in pancreas sections of Flox and βIRBKO mice. Bar, 100 μm or 50 μm.

(H) Quantitative analysis of IHC staining in (G) according to the average integrated optical density per area (IOD/Area). (I) Relative expression levels of *Ins1* in isolated islets of Flox and βIRBKO mice (n = 6 animals). All measurements were conducted with male mice after 24 weeks of HFD. Data are presented as mean ± SEM. Statistical analysis is performed using a Student's t test and statistical significance is shown as $*p < 0.05$, $**p < 0.01$, and $***p < 0.001$.

phosphorylation level of eIF2α (Figures 5J and 5L). Hence, the downregulation of eIF4G1 appears to underlie the decreased CPE in IRB-deficient β cells.

β cell IRB deficiency affects *eIF4G1* expression through transcription factor SREBP1-N

Islet transcriptomics of βIRBKO and Flox mice revealed 1,344 up-regulated genes and 330 down-regulated genes, among which a significant upregulation of a master lipid metabolism regulator, SREBP1, caught our attention (Figures 6A and 6B). We confirmed the increase of *SREBP1* mRNA expression in primary islets of βIRBKO mice (Figure 6C). Notably, not only the amount of full-length SREBP1 (SREBP1-FL) increased but also the level of active SREBP1 mature nuclear form (SREBP1-N) was significantly elevated (Figures 6D–6F) in the knockout mice. Studies have shown that SREBP1 impairs β cell function by inhibiting pancreatic and duodenal homeobox 1 (Pdx-1) transcription.[33] However, we did not detect any change in Pdx-1 expression at both mRNA and protein levels in βIRBKO mice (Figures S5A–S5D).

Through JASPAR database prediction, we identified three SREBP1-responsive sites (SRE) in the eIF4G1 promoter region (Figure S6A). We mutated three SRE sites simultaneously in the eIF4G1-MUT construct and performed luciferase reporter assay in HEK293T cells to detect the transcriptional regulation of eIF4G1 by SREBP1. Luciferase activity driven by eIF4G1's promoter (eIF4G1-WT) is suppressed by overexpression of SREBP1(Figure 6G). In contrast, SREBP1 does not inhibit luciferase activity when driven by a mutated eIF4G1's promoter defective in SREBP1 binding (Figure 6G). In addition, we extracted pancreatic proteins from the global *SREBP1c* null mice (*SREBP1c*$^{-/-}$). In association with the loss of the active SREBP1-N form, the protein level of eIF4G1 was significantly increased in *SREBP1c*$^{-/-}$ mice (Figures 6H–6J). These results indicate that SREBP1 exerts a transcriptional repressive effect on the eIF4G1 gene.

To further understand this unexpected regulation of eIF4G1 by SREBP1, we treated isolated islets with fatostatin hydrobromide, a specific SREBP activation inhibitor, which inhibits the ER-Golgi translocation of SREBPs by binding to SREBP cleavage-activating protein (SCAP).[34] As expected, fatostatin treatment of isolated islets at 10 μM significantly reduced the SREBP1-N level (Figure 6K). Fatostatin treatment did not affect proinsulin content or eIF4G1 levels in the Flox control islets. However, it completely normalized the elevation of proinsulin levels as well as the increased P/I ratio in βIRBKO mice under both low and high glucose environments (Figures 6L and 6M). Supportively, eIF4G1 was restored, together with CPE (Figures 6N and 6O). More importantly, the defect in the SG maturation in IRB-deficient β cells was rescued by fatostatin treatment, as revealed by TEM (Figure 6P).

SREBP1 is a key transcription factor for lipid metabolism. There are two SRE binding sites in the promoter region of the *fatty acid synthase* (*FASN*) gene, which enables SREBPs to regulate the transcription of FASN.[35] Consistently, we found that in IRB-deficient β cells, *FASN* gene expression showed an increasing trend, and the protein level was also significantly up-regulated (Figures 6Q–6S). These data indicate that upregulation of SREBP1-N may cause lipotoxic damage to β cells.

β cell IRB loss elevates IRS-1 level to increase SREBP1-N stability

It has been reported that the mammalian target of rapamycin (mTOR) pathway is involved in the regulation of SREBPs, including processes such as gene transcription, cleavage of full-length precursor proteins into mature activated forms, protein entry into the nucleus and binding to target gene promoters.[36] However, we did not detect any significant upregulation of mTOR and p70 ribosomal protein S6 kinase (p70S6K) phosphorylation in the islets of βIRBKO mice after 24 weeks of HFD feeding (Figures 7A–7C). At the same time, the expression of *SCAP* and *insulin-induced gene 1/2* (*Insig1/2*) involved in SREBP1-FL cleavage activation was not significantly altered at the mRNA level in βIRBKO mouse islets (Figure 7D). However, both mRNA and protein levels of insulin receptor substrate 1 (IRS-1) were up-regulated (Figures 7E–7G). In contrast to elevated insulin-like growth factor 1 receptor (IGF1R) expression in the βIRKO mouse model,[12] we found that IGF1R was down-regulated in the βIRBKO mouse model (Figures 7F and 7H). Due to the high affinity of IRA and proinsulin, excessive proinsulin raises the levels of ERK phosphorylation (Figures 7I and 7J) through IRS-1 in an autocrine manner via IRA.[9]

Due to the nature of IRA/IRB splicing events, it is technically difficult to knock out or knock down IRA directly. We managed to manipulate IRA level indirectly by altering the IRA/IRB alternative splicing regulator CUGBP1 to regulate the IRA/IRB ratio in the MIN6 cell line.[37] CUGBP1 siRNA reduced the IRA/IRB ratio as well as the phosphorylation level of ERK (Figures S7A–S7C). Consistently, CUGBP1 overexpression led to an increase in the IRA/IRB ratio and ERK phosphorylation (Figures S7D–S7F). These data corroborate the aforementioned results from β cells of βIRBKO mice (Figures 7I and 7J).

SREBP-N is highly unstable and is rapidly degraded by the ubiquitin-proteasome pathway,[38] whereas ERK can directly phosphorylate SREBP1-N at the Ser117 site and thus prevent it from F box and WD repeat domain-containing 7 (FBXW7) mediated ubiquitination for degradation.[39] The increased stability of SREBP1-N in the nucleus will further repress the transcription of the eIF4G1 gene, thereby affecting the processing of proinsulin.

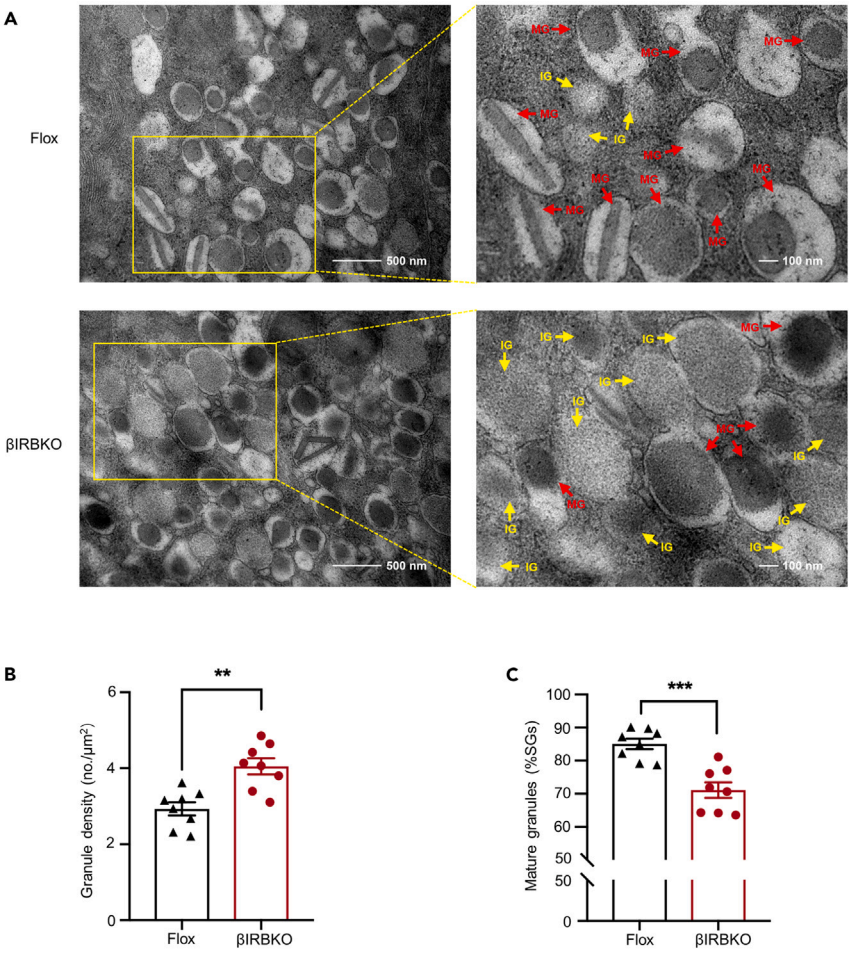

Figure 4. β cell IRB loss impairs the maturation of insulin secretion granules

(A) Representative TEM images of isolated islets of Flox and βIRBKO mice with 50,000 times magnification (left) and 100,000 times magnification (right). Mature granules (MG, characterized by dense core and wide halo) are indicated with red arrows and immature granules (IG, characterized by light content and a narrow halo) are indicated with yellow arrows. Bar, 500 nm or 100 nm.

(B) Quantitation of the density of total secretory granules in TEM images of β cells of Flox and βIRBKO mice (8 β cells in 3 islets per group).

(C) Percentage of mature granules (identify as described in a). All measurements were conducted with male mice after 24 weeks of HFD. Data are presented as mean ± SEM. Statistical analysis is performed using a Student's t test and statistical significance is shown as $^{**}p < 0.01$, and $^{***}p < 0.001$.

DISCUSSION

In this study, we constructed βIRBKO, a β cell-specific IRB knockout mouse model. By studying this unique mouse model, we found that IRB-deficient mice develop hyperproinsulinemia, insulin resistance, and immature insulin SGs accumulated in β cells under high-fat stress. The absence of IRB in β cells disturbs CPE translation by influencing *eIF4G1* expression through the transcription factor SREBP1-N, leading to poor proinsulin processing and exacerbated β cell lipotoxicity. These results suggest a critical role of IRB in protecting β cell function under metabolic stress.

Although the pathological/disease model is missing in human, studies from ours and others do indicate that the ratio of IRA to IRB plays a very important role in human diseases, especially in the islet cells of diabetes and cancers. Data from publicly accessible sources was used to analyze the abundance of INSR across tissues unbiasedly. In a panel of 39 human tissues, the pancreatic islets were abundant with both IR isoforms, and the ratio of IRA/IRB is approximately equal to 1 (Figure S8A). Our previous work found that differential splicing of INSR occurs more frequently in breast cancer than in non-tumor breast tissues and 5∼7-fold higher IRA/IRB ratio is observed in breast cancer tissues.[37] We believe that the IRA/IRB ratio is a dynamically changing process in humans or animals, therefore, an IRB knockout mouse model with a fixed IRA/IRB ratio is instrumental for better understanding their distinct functions. In previous studies, IR knockout mouse models in different genetic backgrounds showed early hyperinsulinemia,[10,11,40] consistent with our current study. Here, we demonstrated that IRB deficiency causes the accumulation of immature insulin SGs in β cells and their release into the blood, which may be the reason for early hyperinsulinemia.

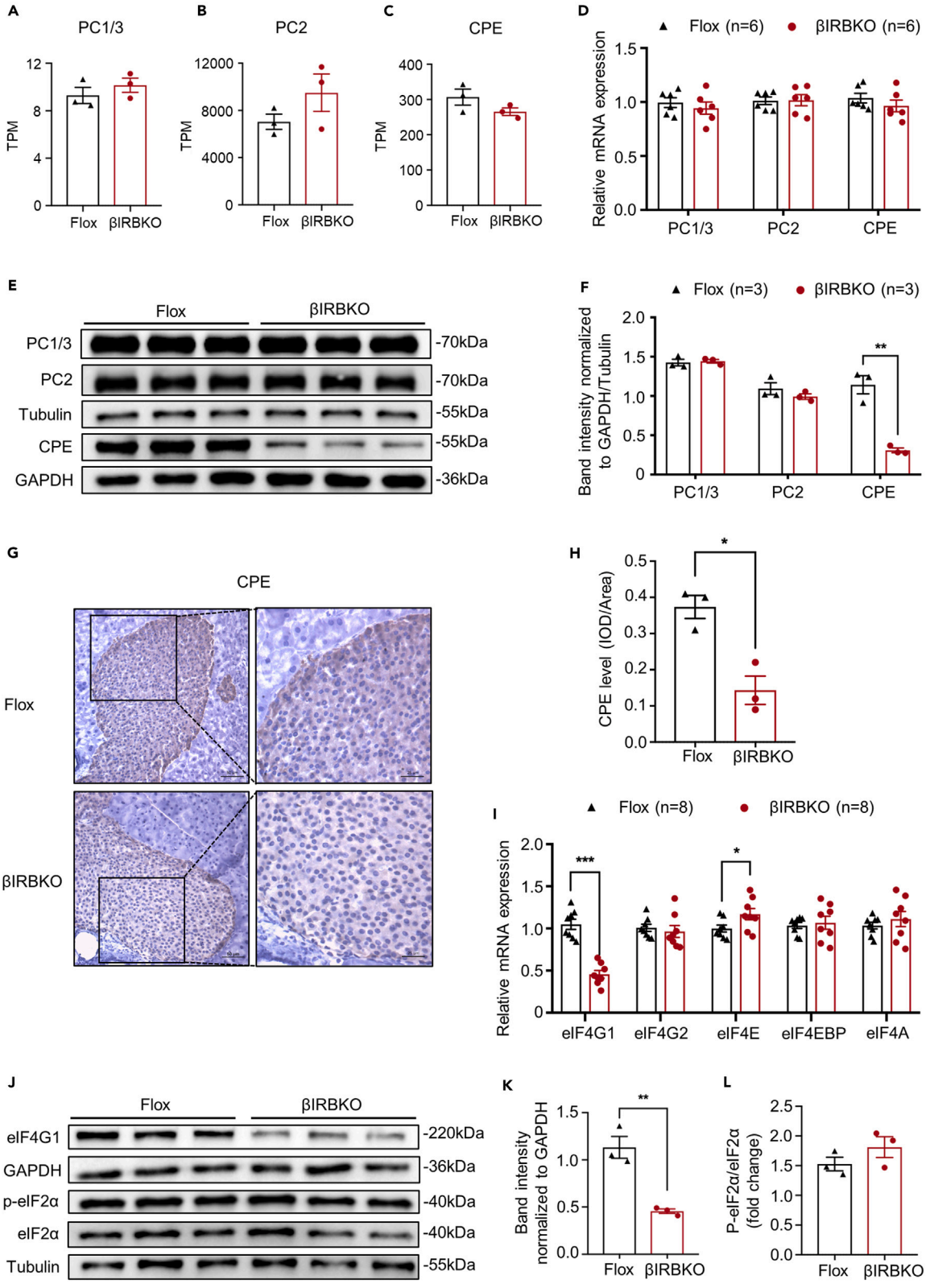
A
PC1/3
TPM
12
8
4
0
Flox
βIRBKO
B
PC2
TPM
12000
8000
4000
0
Flox
βIRBKO
C
CPE
TPM
400
300
200
100
0
Flox
βIRBKO
D
Flox (n=6)
βIRBKO (n=6)
Relative mRNA expression
1.5
1.0
0.5
0.0
PC1/3
PC2
CPE
E
Flox
βIRBKO
PC1/3
PC2
Tubulin
CPE
GAPDH
-70kDa
-70kDa
-55kDa
-55kDa
-36kDa
F
Flox (n=3)
βIRBKO (n=3)
Band intensity normalized to GAPDH/Tubulin
2.0
1.5
1.0
0.5
0
**
PC1/3
PC2
CPE
G
CPE
Flox
βIRBKO
H
CPE level (IOD/Area)
0.5
0.4
0.3
0.2
0.1
0.0
*
Flox
βIRBKO
I
Flox (n=8)
βIRBKO (n=8)
Relative mRNA expression
2.0
1.5
1.0
0.5
0
***
*
eIF4G1
eIF4G2
eIF4E
eIF4EBP
eIF4A
J
Flox
βIRBKO
eIF4G1
GAPDH
p-eIF2α
eIF2α
Tubulin
-220kDa
-36kDa
-40kDa
-40kDa
-55kDa
K
Band intensity normalized to GAPDH
1.5
1.0
0.5
0.0
**
Flox
βIRBKO
L
P-eIF2α/eIF2α (fold change)
2.5
2.0
1.5
1.0
0.5
0.0
Flox
βIRBKO

Figure 5. β cell IRB loss downregulates eIF4G1 expression and CPE translation

(A–C) Expression of *PC1/3* (A), *PC2*(B), and *CPE*(C) in TPM in isolated islets of Flox and βIRBKO mice (n = 3 animals). TPM, Transcripts Per Kilobase of exon model per Million mapped reads.

(D) Relative mRNA expression levels of *PC1/3*, *PC2*, and *CPE* in isolated islets of Flox and βIRBKO mice (n = 6 animals).

(E) Protein levels of PC1/3, PC2, and CPE in isolated islets of Flox or βIRBKO mice.

(F) Quantification of protein expression from (E).

(G) Representative IHC staining images for CPE expression in pancreas sections of Flox and βIRBKO mice. Bar, 50 μm or 25 μm.

(H) Quantitative analysis of IHC staining in (G) and Figure S4A according to the average integrated optical density per area (IOD/Area).

(I) Relative mRNA expression levels of eIF4F-related components in isolated islets of Flox and βIRBKO mice (n = 8 animals).

(J–L) Protein level of eIF4G1, p-eIF2α, and eIF2α in isolated islets of Flox or βIRBKO mice (J) and quantification (K and L). All experiments were conducted with male mice after 24 weeks of HFD. Data are presented as mean ± SEM. Statistical analysis is performed using a Student's t test and statistical significance is shown as $*p < 0.05$, $**p < 0.01$, and $***p < 0.001$.

In Cpe^{fat}/Cpe^{fat} mice with a single S202P mutation abolishing the CPE enzymatic activity, hyperproinsulinemia gradually manifested, and TEM images of β cells showed a dominant occupation of immature granules rich in proinsulin. The pancreatic proinsulin/insulin ratio is 10 times higher in Cpe^{fat}/Cpe^{fat} mice than in the control mice.[41] Similarly, a CPE truncating mutation (c.76_98del) causes morbid obesity and abnormal glucose homeostasis in a female patient.[42] Homozygous nonsense CPE mutations (c.405C>A) cause obesity in three siblings.[43] CPE global knockout mice develop spontaneous obesity, hyperglycemia, insulin resistance, and hyperproinsulinemia.[44] These data are consistent with the endocrine phenotype and β cell dysfunction in βIRBKO mice. Pancreatic β cell-specific CPE knockout mice (β Cpe KO) constructed with Ins1-Cre mice are deficient of mature insulin granules and have elevated proinsulin levels in plasma.[45] However, the glucose tolerance after 16w-HFD and the insulin sensitivity after 20w-HFD were similar to those of Flox mice. These are in contrast to the phenotypes of impaired glucose tolerance and insulin resistance observed in βIRBKO mice after 24w-HFD. The phenotypic discrepancy between the global Cpe KO and β Cpe KO could be explained by two possibilities laid out by Chen et al.[45]: one is that lack of CPE activity in other tissues such as hypothalamus may contribute to obesity and insulin resistance. Another possibility is that other carboxypeptidase such as Cpd is compensating in the pancreatic tissues of β Cpe KO. Nonetheless, the essential role of CPE in proinsulin processing is clear. It is worth to note that the progression of hyperglycemia in β Cpe KO mice was significantly accelerated after low-dose streptozotocin injection, indicating that the loss of CPE will accelerate β cell failure and the progression of diabetes.

Under high-fat stress, pancreatic β cells need to secrete insulin compensatorily, and the excessive secretion demand exposes the failure of proinsulin processing. Due to the low biological activity of proinsulin, blood glucose cannot be effectively controlled, which will further increase the secretory burden of β cells, causing HFD-fed mice to develop metabolic phenotypes such as hyperproinsulinemia, glucose intolerance, and insulin resistance that are different from RC-fed mice.

The speed of mRNA translation initiation is mainly controlled by the thermal stability (lower free energy) of the 5′ hairpin structure: the higher G-C content, the more complex the secondary structure of 5′ UTR, and the more dependent it is on eIF4F to unchain it and bind to the ribosomes.[46] *CPE* has a much higher degree of G-C base pairing and lower ΔG in 5′ UTR than PC1/3, resulting in a more stable hairpin structure and thus is more dependent on eIF4F. Our data demonstrated that only eIF4G1 was down-regulated among the components of eIF4F in the βIRBKO cells. eIF4G1 is a large scaffolding protein bridging mRNA and ribosome, and its decline may directly affect the translation initiation process of eIF4F to CPE.[47] Overexpression of eIF4G1, a substrate of OGlcNAc transferase (OGT), in the islets of βOGTKO increased CPE levels and completely reversed hyperproinsulinemia.[48] Our data provide further evidence of a tight link between eIF4G1 and CPE translation.

Insulin content in islets of βIRBKO mice was significantly increased (Figures 3E, S3B, and S3C), *Ins1* transcription was enhanced (Figure 3I), and SGs density was increased (Figure 4B). It is reasonable to speculate that impaired proinsulin processing capacity is the direct cause of hyperinsulinemia in βIRBKO mice. It leads to the accumulation of many intermediates in cells and release into the circulation, causing insulin resistance and glucose homeostasis imbalance in peripheral tissues, stimulating β cells to increase insulin synthesis. Ultimately, incompetent proinsulin processing leads to β cell overload and a vicious cycle in βIRBKO mice. Leibiger et al. discovered the involvement of IRA in *Ins1* transcription and IRB in *GCK* transcription by overexpressing IRA/IRB in isolated islets from βIRKO mice and in the HIT cell line.[13] Although we did not detect differences in the expression of GCK and GLUT2, their study implies that the two IR isoforms in β cells reflect the selectivity of insulin signaling through different signaling pathways.

SREBP1, a center regulator of lipid metabolism, plays a crucial role in governing the transcription of various lipid synthesis genes, and the excessive expression of SREBP1 has been found to detrimentally impact the functionality of β cells.[49] In this context, we establish a connection between lipid metabolism and glucose metabolism by elucidating the influence of SREBP1 on proinsulin processing. This discovery unveils an additional detrimental effect of lipotoxicity on β cells.

Both discrepancy and similarity in the phenotypes and molecular mechanisms can be found in the βIRBKO model compared to mice with complete knockout of IR in β cell. For example, we found impaired proinsulin processing and hyperinsulinemia in βIRBKO mice, consistent with Liew et al. study and Skovso et al. work, respectively.[12,50] However, relatively weak circulating proinsulin levels are detected, and levels of IGF1R, Pdx-1, and SCAP/Insig expression in βIRBKO mice are distinct from βIRKO.[12] A reasonable explanation for these differences has been given as the remaining IRA could still bind to the proinsulin with higher affinity, mediating the stabilization of SREBP1-N through enhanced ERK activity and forming a feedback loop on proinsulin processing.[9]

In conclusion, we found that loss of IRB in β cells under high-fat stress inhibits the expression of the eIF4G1 through the transcription-repressive function of SREBP1-N, resulting in a blocked translation initiation of CPE mediated by eIF4G1, which impaired the processing

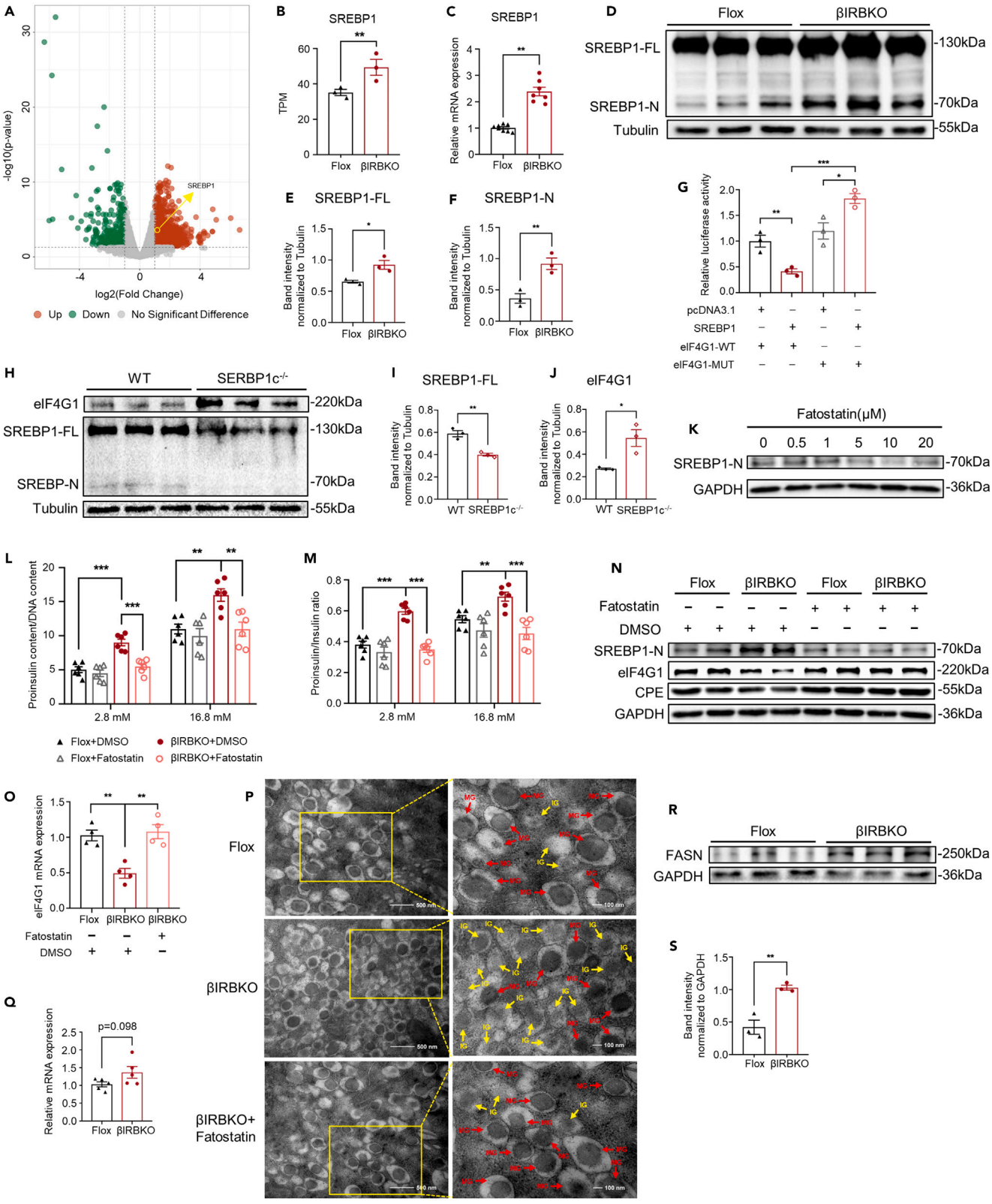
A
-log10(p-value)
log2(Fold Change)
SREBP1
Up
Down
No Significant Difference
B
SREBP1
TPM
Flox
βIRBKO
C
SREBP1
Relative mRNA expression
Flox
βIRBKO
D
Flox
βIRBKO
SREBP1-FL
SREBP1-N
Tubulin
-130kDa
-70kDa
-55kDa
E
SREBP1-FL
Band intensity normalized to Tubulin
Flox
βIRBKO
F
SREBP1-N
Band intensity normalized to Tubulin
Flox
βIRBKO
G
Relative luciferase activity
pcDNA3.1
SREBP1
eIF4G1-WT
eIF4G1-MUT
H
WT
SERBP1c-/-
eIF4G1
SREBP1-FL
SREBP-N
Tubulin
-220kDa
-130kDa
-70kDa
-55kDa
I
SREBP1-FL
Band intensity normalized to Tubulin
WT
SREBP1c-/-
J
eIF4G1
Band intensity normalized to Tubulin
WT
SREBP1c-/-
K
Fatostatin(μM)
0
0.5
1
5
10
20
SREBP1-N
GAPDH
-70kDa
-36kDa
L
Proinsulin content/DNA content
2.8 mM
16.8 mM
Flox+DMSO
βIRBKO+DMSO
Flox+Fatostatin
βIRBKO+Fatostatin
M
Proinsulin/Insulin ratio
2.8 mM
16.8 mM
N
Flox
βIRBKO
Flox
βIRBKO
Fatostatin
DMSO
SREBP1-N
eIF4G1
CPE
GAPDH
-70kDa
-220kDa
-55kDa
-36kDa
O
eIF4G1 mRNA expression
Flox
βIRBKO
βIRBKO
Fatostatin
DMSO
P
Flox
βIRBKO
βIRBKO+
Fatostatin
MG
IG
MC
500 nm
100 nm
Q
p=0.098
Relative mRNA expression
Flox
βIRBKO
R
Flox
βIRBKO
FASN
GAPDH
-250kDa
-36kDa
S
Band intensity normalized to GAPDH
Flox
βIRBKO

Figure 6. β cell IRB deficiency upregulates SREBP1 leading to the accumulation of proinsulin in β cells

(A) Volcano plots illustrating significantly differentially expressed genes (Fold change >1, adjusted *p*-value <0.05). Red dots indicate significantly up-regulated genes, and green dots represent significantly down-regulated genes.

(B) Expression of *SREBP1* in TPM in isolated islets of Flox and βIRBKO mice (*n* = 3 animals). TPM, Transcripts Per Kilobase of exon model per Million mapped reads.

(C) Relative mRNA expression levels of *SREBP1* in isolated islets of Flox and βIRBKO mice (n = 7–8 animals).

(D–F) Protein levels of full-length SREBP1 and nuclear SREBP1 in isolated islets of Flox or βIRBKO mice (D) with quantification shown in (E and F).

(G) Luciferase reporter assay in HEK293T cells transfected with pcDNA3.1, pcDNA3.1-SERBP1, wild-type eIF4G1 promoter (eIF4G1-WT), and mutated (eIF4G1-MUT) plasmid. Values are expressed as relative luciferase activity normalized to cotransfected renilla luciferase activity.

(H–J) Protein levels of eIF4G1, full-length SREBP1, and nuclear SREBP1 in WT or *SERBP1c*$^{-/-}$ mice (H) and quantification (I and J).

(K) Protein levels of nuclear SREBP1 in isolated islets treated with 0-20 μM fatostatin for 24 h.

(L and M) Proinsulin content (L) and proinsulin/insulin ratio (M) measured with ELISA normalized to DNA content in isolated islets of Flox and βIRBKO mice (*n* = 6 animals). Isolated islets were treated with 10 μM fatostatin for 24 h, and then stimulated with 2.8 mM or 16.8 mM glucose for 1 h.

(N) Protein levels of nuclear SREBP1, eIF4G1, and CPE in isolated islets treated with 10 μM fatostatin for 24 h of Flox and βIRBKO mice.

(O) Relative mRNA expression levels of *eIF4G1* in isolated islets treated with 10 μM fatostatin for 24 h of Flox and βIRBKO mice (*n* = 4 animals).

(P) Representative TEM images of isolated islets treated with 10 μM fatostatin for 24 h from Flox and βIRBKO mice with 50,000 times magnification (left) and 100,000 times magnification (right). Mature granules (characterized by dense core and wide halo) are indicated with red arrows and immature granules (characterized by light content and a narrow halo) are indicated with yellow arrows. Bar, 500 nm or 100 nm.

(Q) Relative mRNA expression levels of *FASN* in isolated islets from Flox and βIRBKO mice (*n* = 5 animals).

(R and S) Protein levels of FASN in isolated islets of Flox or βIRBKO mice (R) with quantification shown in (S).All experiments were conducted with male mice after 24 weeks of HFD. Data are presented as mean ± SEM. Statistical analysis is performed using a Student's t test and statistical significance is shown as *$p < 0.05$, **$p < 0.01$, and ***$p < 0.001$.

of proinsulin. βIRBKO mice exhibited insulin resistance, hyperinsulinemia, and hyperproinsulinemia. Excessive autocrine proinsulin raises the ERK phosphorylation levels through IRA to prevent the degradation of SREBP1-N and then forms a feedback loop in βIRBKO mice (Figure 8A). Collectively, our findings provide evidence for the tight regulation of IRB in the processing of proinsulin and in safeguarding β cells against lipotoxicity in the context of obesity.

Limitations of the study

Our study on IRA/IRB's distinct roles in insulin processing and protecting β cells from lipotoxicity in obesity is not complete due to the lack of βIRAKO mouse model. IRA-specific KO model would be a great complement to the IRB KO and would provide a full picture of each isoform's distinct functions. Unfortunately, due to the nature of IRA/IRB splicing, it is almost impossible to make a true IRA KO. Also, all our experiments were performed with male mice. Therefore, we could not rule out the possibility that some of the phenotypes we observed with βIRBKO might be sex specific.

STAR★METHODS

Detailed methods are provided in the online version of this paper and include the following:

- KEY RESOURCES TABLE
- RESOURCE AVAILABILITY
  - Lead contact
  - Materials availability
  - Data and code availability
- EXPERIMENTAL MODEL AND STUDY PARTICIPANT DETAILS
  - Animal studies
- METHOD DETAILS
  - Cell culture and transfection
  - Plasmid construction
  - Transcriptomics sample preparation, library construction, and sequencing
  - Sequencing data processing and analysis
  - GTT, ITT and GSIS analysis
  - Islet isolation and culture
  - Insulin and proinsulin measure using ELISA method
  - RT-PCR analysis
  - Protein extraction and Western blotting
  - Immunohistochemistry
  - TEM and images analysis
  - Luciferase reporter assays
- QUANTIFICATION AND STATISTICAL ANALYSIS

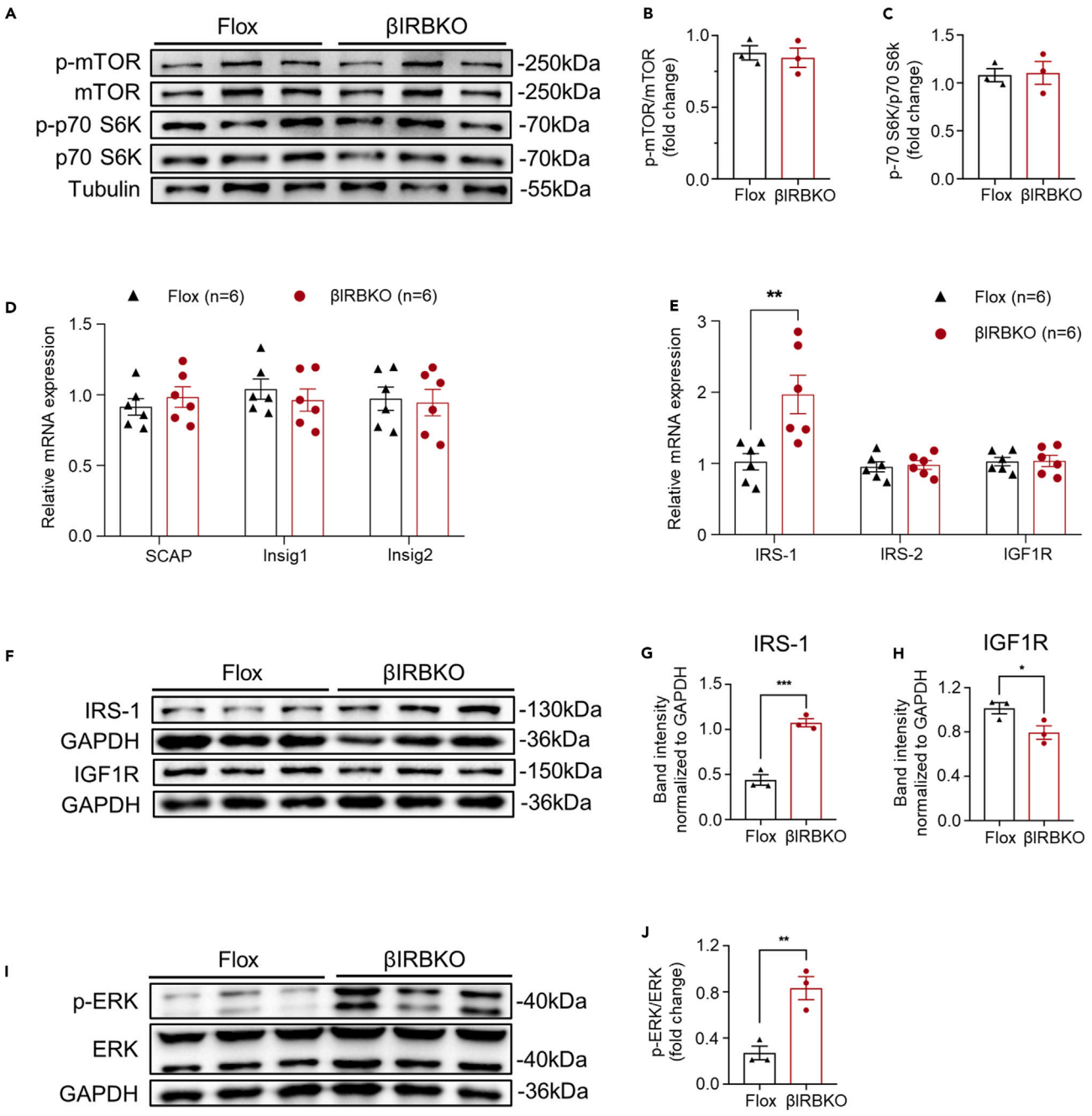

Figure 7. β cell IRB loss elevates IRS-1 level to increase SREBP1-N stability

(A–C) Protein levels of *p*-mTOR, mTOR, p-p70S6K, and p70S6K in isolated islets of Flox or βIRBKO mice (A) and quantification of phosphorylation level of tested proteins (B and C).

(D) Relative mRNA expression levels of *SCAP*, *Insig1*, and *Insig2* in isolated islets from Flox and βIRBKO mice ($n = 6$ animals).

(E) Relative mRNA expression levels of *IRS-1*, *IRS-2i*, and *IGF1R* in isolated islets from Flox and βIRBKO mice ($n = 6$ animals).

(F–H) Protein levels of IRS-1 and IGF1R (F) in isolated islets from Flox or βIRBKO mice with quantification shown in (G and H).

(I and J) Protein levels of *p*-ERK and ERK in isolated islets from Flox or βIRBKO mice (I) and quantification of phosphorylation level of *p*-ERK (J). All experiments were conducted with male mice after 24 weeks of HFD. Data are presented as mean ± SEM. Statistical analysis is performed using a Student's t test and statistical significance is shown as $*p < 0.05$, $**p < 0.01$, and $***p < 0.001$.

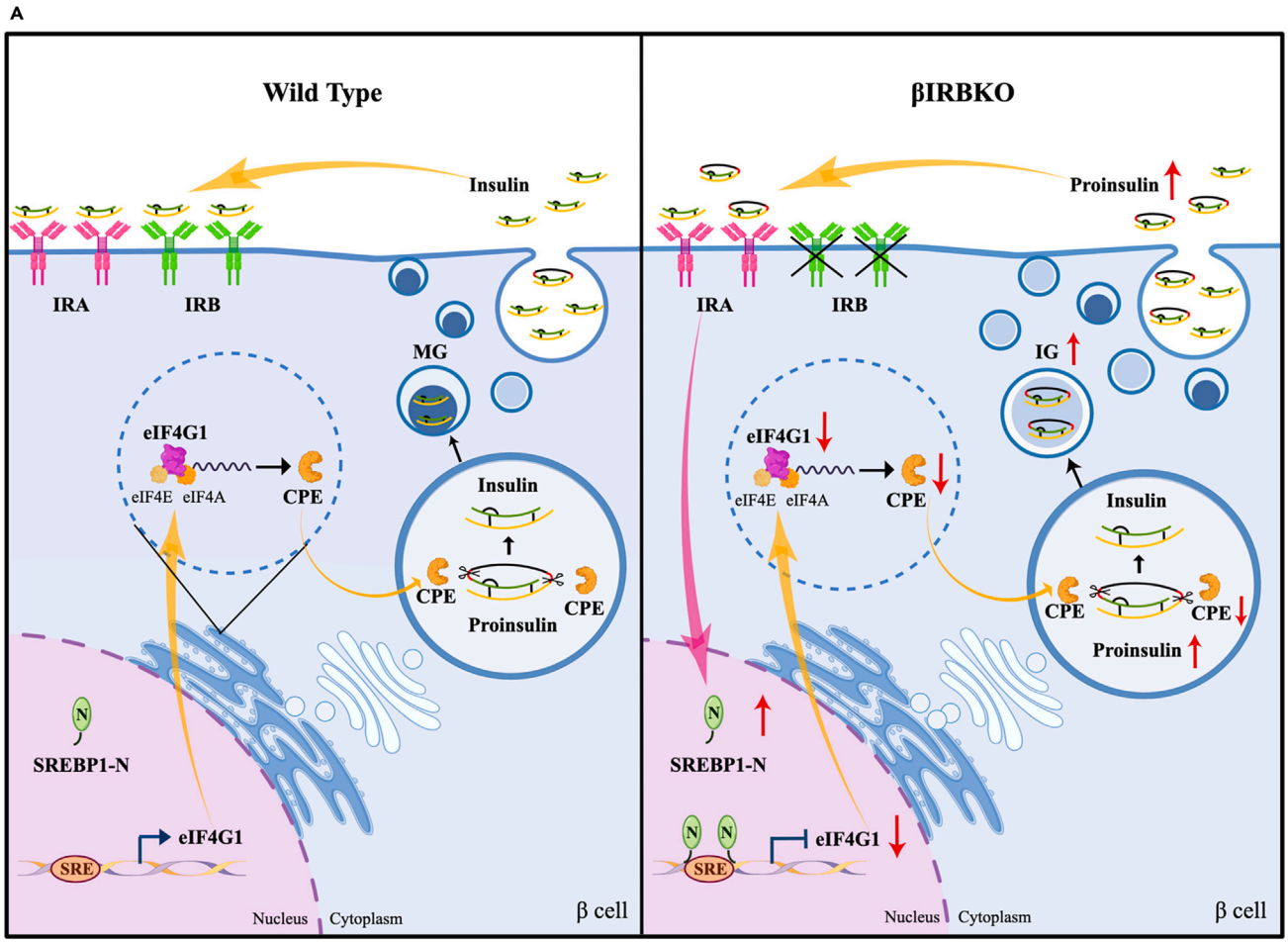

Figure 8. Model on how IRB deletion impairs proinsulin processing in pancreatic β cells

(A) In contrast to the wild type, β cells that lose IRB have only IRA. Proinsulin has a higher affinity for IRA, which leads to up-regulated levels of SREBP1-N in the nucleus. SREBP1-N binds to the promoter of *eIF4G1* to repress its expression. The decrease in eIF4G1 prevents the translation of CPE and reduces its level, leading to impaired processing of proinsulin, which is secreted extracellularly in the form of IGs. Proinsulin then binds to IRA to form a feedback loop. The diagram was drawn using Figdraw.

SUPPLEMENTAL INFORMATION

Supplemental information can be found online at https://doi.org/10.1016/j.isci.2024.110017.

ACKNOWLEDGMENTS

This work was supported by the Ministry of Science and Technology of the People's Republic of China (2021YFF0702100, 2021YFA0805100, and 2022YFE0132200), the National Natural Science Foundation of China (no.81471000, no.31871163, no.82370866) and the Talent Cultivation Fund Project of Dalian Medical University (no.508027).

AUTHOR CONTRIBUTIONS

M.J. and N.W. designed the experiments and wrote the manuscript. M.J. and Y.Z. performed experiments and collected and analyzed data. J.Z. helped to analyze and interpret the data. Y.L. and N.W. performed animal breeding. X.Y., H.Z., Y.L., and C.L. assisted in the experiment. Y.G. helped with *SERBP1c*$^{-/-}$ mice and experiment. Y.W., W.Z., and B.L. contributed to the conception of research and study design and critically revised the article for important intellectual content. All authors were involved in editing and reviewing the manuscript. Y.W. is the guarantor of this work. All authors approved the final version to be published.

DECLARATION OF INTERESTS

The authors declare no competing interests.

Received: October 30, 2023
Revised: March 27, 2024
Accepted: May 14, 2024
Published: May 17, 2024

REFERENCES

1. Wright, C.J., Smith, C.W.J., and Jiggins, C.D. (2022). Alternative splicing as a source of phenotypic diversity. Nat. Rev. Genet. *23*, 697–710.
2. Wang, E.T., Sandberg, R., Luo, S., Khrebtukova, I., Zhang, L., Mayr, C., Kingsmore, S.F., Schroth, G.P., and Burge, C.B. (2008). Alternative isoform regulation in human tissue transcriptomes. Nature *456*, 470–476.
3. Johnson, J.M., Castle, J., Garrett-Engele, P., Kan, Z., Loerch, P.M., Armour, C.D., Santos, R., Schadt, E.E., Stoughton, R., and Shoemaker, D.D. (2003). Genome-wide survey of human alternative pre-mRNA splicing with exon junction microarrays. Science *302*, 2141–2144.
4. Wang, G.S., and Cooper, T.A. (2007). Splicing in disease: disruption of the splicing code and the decoding machinery. Nat. Rev. Genet. *8*, 749–761.
5. Seino, S., Seino, M., Nishi, S., and Bell, G.I. (1989). Structure of the human insulin receptor gene and characterization of its promoter. SA *86*, 114–118.
6. Belfiore, A., Malaguarnera, R., Vella, V., Lawrence, M.C., Sciacca, L., Frasca, F., Morrione, A., and Vigneri, R. (2017). Insulin Receptor Isoforms in Physiology and Disease: An Updated View. Endocr. Rev. *38*, 379–431.
7. Frasca, F., Pandini, G., Scalia, P., Sciacca, L., Mineo, R., Costantino, A., Goldfine, I.D., Belfiore, A., and Vigneri, R. (1999). Insulin receptor isoform A, a newly recognized, high-affinity insulin-like growth factor II receptor in fetal and cancer cells. Mol. Cell Biol. *19*, 3278–3288.
8. Savkur, R.S., Philips, A.V., and Cooper, T.A. (2001). Aberrant regulation of insulin receptor alternative splicing is associated with insulin resistance in myotonic dystrophy. Nat. Genet. *29*, 40–47.
9. Malaguarnera, R., Sacco, A., Voci, C., Pandini, G., Vigneri, R., and Belfiore, A. (2012). Proinsulin binds with high affinity the insulin receptor isoform A and predominantly activates the mitogenic pathway. Endocrinology *153*, 2152–2163.
10. Kulkarni, R.N., Brüning, J.C., Winnay, J.N., Postic, C., Magnuson, M.A., and Kahn, C.R. (1999). Tissue-specific knockout of the insulin receptor in pancreatic beta cells creates an insulin secretory defect similar to that in type 2 diabetes. Cell *96*, 329–339.
11. Okada, T., Liew, C.W., Hu, J., Hinault, C., Michael, M.D., Krtzfeldt, J., Yin, C., Holzenberger, M., Stoffel, M., and Kulkarni, R.N. (2007). Insulin receptors in beta-cells are critical for islet compensatory growth response to insulin resistance. SA *104*, 8977–8982.
12. Liew, C.W., Assmann, A., Templin, A.T., Raum, J.C., Lipson, K.L., Rajan, S., Qiang, G., Hu, J., Kawamori, D., Lindberg, I., et al. (2014). Insulin regulates carboxypeptidase E by modulating translation initiation scaffolding protein eIF4G1 in pancreatic β cells. SA *111*, E2319–E2328.
13. Leibiger, B., Leibiger, I.B., Moede, T., Kemper, S., Kulkarni, R.N., Kahn, C.R., de Vargas, L.M., and Berggren, P.O. (2001). Selective insulin signaling through A and B insulin receptors regulates transcription of insulin and glucokinase genes in pancreatic beta cells. Mol. Cell *7*, 559–570.
14. Nevado, C., Valverde, A.M., and Benito, M. (2006). Role of insulin receptor in the regulation of glucose uptake in neonatal hepatocytes. Endocrinology *147*, 3709–3718.
15. Escribano, O., Gómez-Hernández, A., Díaz-Castroverde, S., Nevado, C., García, G., Otero, Y.F., Perdomo, L., Beneit, N., and Benito, M. (2015). Insulin receptor isoform A confers a higher proliferative capability to pancreatic beta cells enabling glucose availability and IGF-I signaling. Mol. Cell. Endocrinol. *409*, 82–91.
16. Magnuson, M.A., and Osipovich, A.B. (2013). Pancreas-specific Cre driver lines and considerations for their prudent use. Cell Metab. *18*, 9–20.
17. Li, L., Gao, L., Wang, K., Ma, X., Chang, X., Shi, J.H., Zhang, Y., Yin, K., Liu, Z., Shi, Y., et al. (2016). Knockin of Cre Gene at Ins2 Locus Reveals No Cre Activity in Mouse Hypothalamic Neurons. Sci. Rep. *6*, 20438.
18. Parween, S., Eriksson, M., Nord, C., Kostromina, E., and Ahlgren, U. (2017). Spatial and quantitative datasets of the pancreatic β-cell mass distribution in lean and obese mice. Sci. Data *4*, 170031.
19. Alarcon, C., Boland, B.B., Uchizono, Y., Moore, P.C., Peterson, B., Rajan, S., Rhodes, O.S., Noske, A.B., Haataja, L., Arvan, P., et al. (2016). Pancreatic β-Cell Adaptive Plasticity in Obesity Increases Insulin Production but Adversely Affects Secretory Function. Diabetes *65*, 438–450.
20. Pfützner, A., Kunt, T., Hohberg, C., Mondok, A., Pahler, S., Konrad, T., Lübben, G., and Forst, T. (2004). Fasting intact proinsulin is a highly specific predictor of insulin resistance in type 2 diabetes. Diabetes Care *27*, 682–687.
21. Nagi, D.K., Hendra, T.J., Ryle, A.J., Cooper, T.M., Temple, R.C., Clark, P.M., Schneider, A.E., Hales, C.N., and Yudkin, J.S. (1990). The relationships of concentrations of insulin, intact proinsulin and 32-33 split proinsulin with cardiovascular risk factors in type 2 (non-insulin-dependent) diabetic subjects. Diabetologia *33*, 532–537.
22. Haffner, S.M., Mykkänen, L., Valdez, R.A., Stern, M.P., Holloway, D.L., Monterrosa, A., and Bowsher, R.R. (1994). Disproportionately increased proinsulin levels are associated with the insulin resistance syndrome. J. Clin. Endocrinol. Metab. *79*, 1806–1810.
23. Kahn, S.E., Leonetti, D.L., Prigeon, R.L., Boyko, E.J., Bergstrom, R.W., and Fujimoto, W.Y. (1995). Proinsulin as a marker for the development of NIDDM in Japanese-American men. Diabetes *44*, 173–179.
24. Liu, M., Wright, J., Guo, H., Xiong, Y., and Arvan, P. (2014). Proinsulin entry and transit through the endoplasmic reticulum in pancreatic beta cells. Vitam. Horm. *95*, 35–62.
25. Liu, M., Weiss, M.A., Arunagiri, A., Yong, J., Rege, N., Sun, J., Haataja, L., Kaufman, R.J., and Arvan, P. (2018). Biosynthesis, structure, and folding of the insulin precursor protein. Diabetes Obes. Metab. *20*, 28–50.
26. Furuta, M., Yano, H., Zhou, A., Rouillé, Y., Holst, J.J., Carroll, R., Ravazzola, M., Orci, L., Furuta, H., and Steiner, D.F. (1997). Defective prohormone processing and altered pancreatic islet morphology in mice lacking active SPC2. SA *94*, 6646–6651.
27. Du, W., Zhou, M., Zhao, W., Cheng, D., Wang, L., Lu, J., Song, E., Feng, W., Xue, Y., Xu, P., and Xu, T. (2016). HID-1 is required for homotypic fusion of immature secretory granules during maturation. Elife *5*, e18134.
28. Adam, J., Ramracheya, R., Chibalina, M.V., Ternette, N., Hamilton, A., Tarasov, A.I., Zhang, Q., Rebelato, E., Rorsman, N.J.G., Martín-Del-Río, R., et al. (2017). Fumarate Hydratase Deletion in Pancreatic β Cells Leads to Progressive Diabetes. Cell Rep. *20*, 3135–3148.
29. Leu, S.Y., Kuo, L.H., Weng, W.T., Lien, I.C., Yang, C.C., Hsieh, T.T., Cheng, Y.N., Chien, P.H., Ho, L.C., Chen, S.H., et al. (2020). Loss of EGR-1 uncouples compensatory responses of pancreatic β cells. Theranostics *10*, 4233–4249.
30. Chen, Y.C., Taylor, A.J., and Verchere, C.B. (2018). Islet prohormone processing in health and disease. Diabetes Obes. Metab. *20*, 64–76.
31. Preiss, T., and Hentze, M.W. (1999). From factors to mechanisms: translation and translational control in eukaryotes. Curr. Opin. Genet. Dev. *9*, 515–521.
32. Gradi, A., Svitkin, Y.V., Imataka, H., and Sonenberg, N. (1998). Proteolysis of human eukaryotic translation initiation factor eIF4GII, but not eIF4GI, coincides with the shutoff of host protein synthesis after poliovirus infection. SA *95*, 11089–11094.
33. Amemiya-Kudo, M., Oka, J., Takeuchi, Y., Okazaki, H., Yamamoto, T., Yahagi, N., Matsuzaka, K., Okazaki, S., Osuga, J.i., Yamada, N., et al. (2011). Suppression of the pancreatic duodenal homeodomain transcription factor-1 (Pdx-1) promoter by sterol regulatory element-binding protein-1c (SREBP-1c). J. Biol. Chem. *286*, 27902–27914.
34. Kamisuki, S., Mao, Q., Abu-Elheiga, L., Gu, Z., Kugimiya, A., Kwon, Y., Shinohara, T., Kawazoe, Y., Sato, S.i., Asakura, K., et al. (2009). A small molecule that blocks fat synthesis by inhibiting the activation of SREBP. Chem. Biol. *16*, 882–892.
35. Bennett, M.K., Lopez, J.M., Sanchez, H.B., and Osborne, T.F. (1995). Sterol regulation of fatty acid synthase promoter. Coordinate feedback regulation of two major lipid pathways. J. Biol. Chem. *270*, 25578–25583.
36. Shimano, H., and Sato, R. (2017). SREBP-regulated lipid metabolism: convergent physiology - divergent pathophysiology. Nat. Rev. Endocrinol. *13*, 710–730.
37. Huang, G., Song, C., Wang, N., Qin, T., Sui, S., Obr, A., Zeng, L., Wood, T.L., Leroith, D., Li, M., and Wu, Y. (2020). RNA-binding protein

CUGBP1 controls the differential INSR splicing in molecular subtypes of breast cancer cells and affects cell aggressiveness. Carcinogenesis *41*, 1294–1305.

38. Bengoechea-Alonso, M.T., Punga, T., and Ericsson, J. (2005). Hyperphosphorylation regulates the activity of SREBP1 during mitosis. SA *102*, 11681–11686.
39. Roth, G., Kotzka, J., Kremer, L., Lehr, S., Lohaus, C., Meyer, H.E., Krone, W., and Müller-Wieland, D. (2000). MAP kinases Erk1/2 phosphorylate sterol regulatory element-binding protein (SREBP)-1a at serine 117 in vitro. J. Biol. Chem. *275*, 33302–33307.
40. Otani, K., Kulkarni, R.N., Baldwin, A.C., Krutzfeldt, J., Ueki, K., Stoffel, M., Kahn, C.R., and Polonsky, K.S. (2004). Reduced beta-cell mass and altered glucose sensing impair insulin-secretory function in betaIRKO mice. Am. J. Physiol. Endocrinol. Metab. *286*, E41–E49.
41. Naggert, J.K., Fricker, L.D., Varlamov, O., Nishina, P.M., Rouille, Y., Steiner, D.F., Carroll, R.J., Paigen, B.J., and Leiter, E.H. (1995). Hyperproinsulinaemia in obese fat/fat mice associated with a carboxypeptidase E mutation which reduces enzyme activity. Nat. Genet. *10*, 135–142.
42. Alsters, S.I.M., Goldstone, A.P., Buxton, J.L., Zekavati, A., Sosinsky, A., Yiorkas, A.M., Holder, S., Klaber, R.E., Bridges, N., van Haelst, M.M., et al. (2015). Truncating Homozygous Mutation of Carboxypeptidase E (CPE) in a Morbidly Obese Female with Type 2 Diabetes Mellitus, Intellectual Disability and Hypogonadotrophic Hypogonadism. PLoS One *10*, e0131417.
43. Durmaz, A., Aykut, A., Atik, T., Özen, S., Ayyıldız Emecen, D., Ata, A., Işık, E., Gökşen, D., Çoğulu, Ö., and Özkınay, F. (2021). A New Cause of Obesity Syndrome Associated with a Mutation in the Carboxypeptidase Gene Detected in Three Siblings with Obesity, Intellectual Disability and Hypogonadotropic Hypogonadism. J. Clin. Res. Pediatr. Endocrinol. *13*, 52–60.
44. Cawley, N.X., Zhou, J., Hill, J.M., Abebe, D., Romboz, S., Yanik, T., Rodriguiz, R.M., Wetsel, W.C., and Loh, Y.P. (2004). The carboxypeptidase E knockout mouse exhibits endocrinological and behavioral deficits. Endocrinology *145*, 5807–5819.
45. Chen, Y.C., Taylor, A.J., Fulcher, J.M., Swensen, A.C., Dai, X.Q., Komba, M., Wrightson, K.L.C., Fok, K., Patterson, A.E., Klein Geltink, R.I., et al. (2023). Deletion of Carboxypeptidase E in β-Cells Disrupts Proinsulin Processing but Does Not Lead to Spontaneous Development of Diabetes in Mice. Diabetes *72*, 1277–1288.
46. Svitkin, Y.V., Pause, A., Haghighat, A., Pyronnet, S., Witherell, G., Belsham, G.J., and Sonenberg, N. (2001). The requirement for eukaryotic initiation factor 4A (eIF4A) in translation is in direct proportion to the degree of mRNA 5′ secondary structure. Rna *7*, 382–394.
47. Gingras, A.C., Raught, B., and Sonenberg, N. (1999). eIF4 initiation factors: effectors of mRNA recruitment to ribosomes and regulators of translation. Annu. Rev. Biochem. *68*, 913–963.
48. Jo, S., Lockridge, A., and Alejandro, E.U. (2019). eIF4G1 and carboxypeptidase E axis dysregulation in O-GlcNAc transferase-deficient pancreatic β-cells contributes to hyperproinsulinemia in mice. J. Biol. Chem. *294*, 13040–13050.
49. Takahashi, A., Motomura, K., Kato, T., Yoshikawa, T., Nakagawa, Y., Yahagi, N., Sone, H., Suzuki, H., Toyoshima, H., Yamada, N., and Shimano, H. (2005). Transgenic mice overexpressing nuclear SREBP-1c in pancreatic beta-cells. Diabetes *54*, 492–499.
50. Skovsø, S., Panzhinskiy, E., Kolic, J., Cen, H.H., Dionne, D.A., Dai, X.Q., Sharma, R.B., Elghazi, L., Ellis, C.E., Faulkner, K., et al. (2022). Beta-cell specific Insr deletion promotes insulin hypersecretion and improves glucose tolerance prior to global insulin resistance. Nat. Commun. *13*, 735.
51. Wick, R.R., Judd, L.M., and Holt, K.E. (2019). Performance of neural network basecalling tools for Oxford Nanopore sequencing. Genome Biol. *20*, 129.
52. De Coster, W., and Rademakers, R. (2023). NanoPack2: population-scale evaluation of long-read sequencing data. Bioinformatics *39*, btad311.
53. Li, H. (2018). Minimap2: pairwise alignment for nucleotide sequences. Bioinformatics *34*, 3094–3100.
54. Danecek, P., Bonfield, J.K., Liddle, J., Marshall, J., Ohan, V., Pollard, M.O., Whitwham, A., Keane, T., McCarthy, S.A., Davies, R.M., and Li, H. (2021). Twelve years of SAMtools and BCFtools. GigaScience *10*, giab008.
55. Pertea, M., Pertea, G.M., Antonescu, C.M., Chang, T.C., Mendell, J.T., and Salzberg, S.L. (2015). StringTie enables improved reconstruction of a transcriptome from RNA-seq reads. Nat. Biotechnol. *33*, 290–295.
56. Love, M.I., Huber, W., and Anders, S. (2014). Moderated estimation of fold change and dispersion for RNA-seq data with DESeq2. Genome Biol. *15*, 550.

STAR★METHODS

KEY RESOURCES TABLE

REAGENT or RESOURCE	SOURCE	IDENTIFIER
Antibodies		
p-AKT	Proteintech	CAT:28731-1-AP
AKT	Proteintech	CAT:10176-2-AP
Proinsulin	Abcam	CAT:ab243141
Insulin	Abclonal	CAT:A19066
PC1/3	Abcam	CAT:ab220363
PCSK2	Proteintech	CAT:10553-1-AP
CPE	Santa Cruz Biotechnology	CAT:sc-393761
eIF4G1	CST	CAT:2858
p-eIF2α	CST	CAT:9721
eIF2α	CST	CAT:9722
Pdx1	Abclonal	CAT:A10173
SREBP1	Abcam	CAT:ab28481
p-mTOR	CST	CAT:2971
mTOR	Proteintech	CAT:28273-1-AP
p-p70 S6K	CST	CAT:9205
p70 S6K	CST	CAT:9202
p-IRS1	Abbkine	CAT:ABP54927
IRS1	Abbkine	CAT:ABP51647
IGF1R	Bioss	CAT:bs-0680R
p-ERK	Abbkine	CAT:ABP0035
ERK	Abbkine	CAT:ABP0085
p-IR	Abbkine	CAT:ABP54910
IR	Abbkine	CAT:ABP54912
p-PI3K	Abbkine	CAT:ABP0163
PI3K	Abbkine	CAT:ABP52199
p-GSK3β	Abbkine	CAT:ABP0037
GSK3β	Abbkine	CAT:ABP51488
GLUT2	Proteintech	CAT:20436-1-AP
GCK	Proteintech	CAT:19666-1-AP
FASN	Proteintech	CAT:10624-2-AP
CUGBP1	Proteintech	CAT:13002-1-AP
Tubulin	Abbkine	CAT:ABL1030
GAPDH	Abbkine	CAT:ABL1021
HRP-Rabbit	Abbkine	CAT:A21020
HRP -Mouse	Abbkine	CAT:A21010
Chemicals, peptides, and recombinant proteins		
Collagenase V	Sigma	CAT:C9263
Fatostatin hydrobromide	MCE	CAT:HY-14452A
Lipofectamine 3000	Invitrogen	CAT:L3000150
Recombinant human insulin	Jiangsu Wanbang Biochemistry Medicine Company	CAT:H10890001

(*Continued on next page*)

Continued

REAGENT or RESOURCE	SOURCE	IDENTIFIER
Critical commercial assays		
Mouse INS ELISA Kit	MSKBIO	CAT:69-21071
Mouse PI ELISA Kit	MSKBIO	CAT:69-21129
Dual Luciferase Reporter Gene Assay Kit	Abbkine	CAT:KTA8010
One-Step gDNA Removal and cDNA Synthesis SuperMix	TransGen Biotech	CAT:AT311
Tip Green qPCR SuperMix kit	TransGen Biotech	CAT:AQ142
BCA Protein Assay Kit	Beyotime	CAT:P0012
Universal ECL Substrate	Abbkine	CAT:BMP3010
Deposited data		
3rd generation sequence data	This paper	GSA:PRJCA025749
Experimental models: Cell lines		
MIN6	Naval Medical University	N/A
HEK293T	Naval Medical University	N/A
Experimental models: Organisms/strains		
Wild type C57BL/6 mouse	The Jackson Laboratory	N/A
db/db mouse	The Jackson Laboratory	N/A
IRB Flox mouse	Institute for Genome Engineered Animal Models of Human Diseases, Dalian Medical University	N/A
Ins2-Cre mouse	Department of Pathophysiology, Naval Medical University	N/A
SREBP1c-null mouse	The Jackson Laboratory	N/A
Software and algorithms		
ImageJ	National Institutes of Health	https://imagej.nih.gov/ij/
GraphPad Prism 9.0	GraphPad Prism Software	https://www.graphpad.com/
Other		
Regular chow diet	Medicience Ltd.	CAT:MD12031
High fat diet	Medicience Ltd.	CAT:MD12033

RESOURCE AVAILABILITY

Lead contact

Further information and requests for resources should be directed to and will be fulfilled by the lead contact, Yingjie Wu (yingjiewu@dmu.edu.cn).

Materials availability

Materials availability will be available upon request from the lead contact.

Data and code availability

- 3rd generation sequence data have been deposited at GSA and are publicly available as of the date of publication. Accession numbers are listed in the key resources table.
- This paper does not report original code.
- Any additional information required to reanalyze the data reported in this paper is available from the lead contact upon request.

EXPERIMENTAL MODEL AND STUDY PARTICIPANT DETAILS

Animal studies

Care and treatment of laboratory animals were in accordance with institutional guidelines and were approved by the Committee on the Ethics of Animal Experiments of Dalian Medical University (permit number AEE19081). IRB Flox mice were generated by inserting two

LoxP sites flanking exon 11 in the pure C57BL/6 background. By crossing IRB Flox mice with Ins2-Cre mice in a C57BL/6 background, βIRBKO mice and their control littermates were obtained. SREBP1c-null mice (SREBP1c$^{-/-}$) were gifted by professor Youfei Guan (from The Jackson Laboratory). All experiments were only performed with male mice aged 3-28 weeks and "n" refers to the number of single animal tested. Adult mice were fed with regular chow (RC) (MD12031, 10 g/100 g fat, Medicience Ltd., China) or HFD (MD12033, 60 g/100 g fat, Medicience Ltd., China) and had free access to water, housed in a temperature- and humidity-controlled room on a 12h light/dark cycle at Specific Pathogen Free Experimental Animal Center of Dalian Medical University. Mice were anesthetized with 1% pentobarbital sodium for glucose stimulated insulin secretion (GSIS) or islet isolation. After CO2 euthanasia, tissues were dissected and weighed, then fixed with 4% paraformaldehyde or snap-frozen in liquid nitrogen before stored at −80°C. The genotyping of mice was performed by PCR using specific primers (Table S1).

METHOD DETAILS

Cell culture and transfection

MIN6 and HEK293T cells were cultured in DMEM medium (Gibco, USA) supplemented with 10% fetal bovine serum (FBS) (Gibco, USA) at 37°C in 5% CO2 incubator. Lipofectamine 3000 (Invitrogen, CA) was used to transfect CUGBP1 small interfering RNAs (siRNAs) and negative control siRNAs (GenePharma, Suzhou, China) as well as plasmid DNA. CUGBP1 siRNA#1: sense: 5′-GGAUGCAUCACCCUAUACATT-3′. Cells were collected 24 h after transfection for PCR and Western blotting.

Plasmid construction

CUGBP1 open reading frame was amplified by PCR and subcloned into the pcDNA3.1 vector (GenePharma, Suzhou, China) at EcoRI and BamHI sites. Wild type (WT) and three SRE site simultaneous deletion mutated (MUT) eIF4G1 promoter (-2000∼+100) was amplified by PCR and subcloned into the pGL4.10 vector (OBiO, Shanghai, China) at BglII and HindIII sites. SREBP1 open reading frame was amplified by PCR and subcloned into the pcDNA3.1 vector at EcoRI sites. All plasmid constructs were sequencing confirmed.

Transcriptomics sample preparation, library construction, and sequencing

Total RNA was extracted using TRIzol™ (Invitrogen™) and enriched for poly(A) mRNA using the NEBNext Poly(A) mRNA Magnetic Isolation Module. Synthesis of cDNA for sequencing followed the strand-switching protocol from Oxford Nanopore Technologies. Briefly, the cDNA-PCR Sequencing kit by Oxford Nanopore (SQK-PCS109) was used to prepare full-length cDNA libraries from the poly(A) mRNAs. Then the cDNA was amplified by PCR for 13-14 cycles with specific barcoded adapters from the Oxford Nanopore PCR Barcoding kit (SQKPBK004). Finally, the 1D sequencing adapter was ligated to the DNA before loading onto a PromethION R9.4.1 flow cell in a PromethION sequencer. MinKNOW was used to run the sequencing.

Sequencing data processing and analysis

DNA bases were called from FAST5 files using ONT Guppy GPU (v5.0.16) in high accuracy mode.[51] Reads with an average Phred quality score lower than 7 were discarded. Raw reads quality was assessed using NanoPlot,[52] and then full-length Nanopore cDNA reads were identified, oriented, and trimmed using Pychopper (v2.4.0) [EPI2ME Labs]. Full-length reads were aligned to the GRCm39 mouse reference genome with minimap2 (v2.17), using default parameters except for -ax splice -uf -k14.[53] The alignment results were converted from SAM to BAM format and the alignment quality was assessed using Samtools (v1.19).[54] Read counting, as well as gene and transcript quantification, were performed using Stringtie2.[55] Gene and transcript count normalization and differential analysis were conducted using the DESeq2 R package.[56] Differentially expressed genes (DEGs) and transcripts were identified based on a fold change > 1 and a false discovery rate (FDR) < 0.05.

GTT, ITT and GSIS analysis

Intraperitoneal (IP) glucose tolerance test (GTT) was performed in overnight-fasted mice with 2.0 g glucose per kg of body weight. The whole-tail vein blood was collected at 0, 15, 30, 60 and 120 min after injection. Blood glucose was measured using a glucose meter (Roch, Switzerland). Intraperitoneal insulin tolerance test (ITT) was performed on 6h-fasted mice with 0.75 unit of insulin (recombinant human insulin, Jiangsu Wanbang Biochemistry Medicine Company, China) per kg of body weight and measured at 0, 15, 30 and 60 min after injection. Mice were fasted overnight to perform *in vivo* GSIS. After anesthesia, blood samples were taken from the eye socket vein at 0, 15, 30, 60 and 120 min after IP injection with 3.0 g glucose per kg of body weight. Serum was separated from whole blood by centrifugation and then used for ELISA.

Islet isolation and culture

Solution preparation

40 mg Type V collagenase (C9263, Sigma, USA) and 1 g bovine serum albumin (BSA) (9048-46-8, Solarbio, China) powder were dissolved in RPMI medium to obtain 50 ml collagenase solution. 10% fetal bovine serum (FBS) (9048-46-8, Solarbio, China) and 1%

Penicillin-Streptomycin (C0222, Beyotime, China) were added into RPMI 1640 medium with L-glutamine (11875, GIBCO, USA) to obtain islet culture solution.

Surgical operation

The abdominal cavity of anesthetized mice, was exposed to locate the major duodenal papilla, which was clamped with surgical clamps on the duodenum wall. A 30G1/2-G needle was inserted into the common bile duct through the joint site of the hepatic duct and the cystic duct under a microscope, and then slowly injected with 3 ml of collagenase solution to expand the pancreas. Pancreas were then removed and placed in a 50 ml tube containing 5 ml of collagenase solution, which was then incubated in a water bath at 37.5°C for 15 min. After incubation, shake the tube by hand to disrupt the pancreas until the suspension becomes homogeneous. The tube was then placed on ice and added 8 ml of islet culture solution to stop digestion. The suspension was then filtered with a cell strainer (70 μm, Falcon, USA). The strainer was turned upside down over a new 10 cm dish and the captured islets were rinsed into the dish with 15 ml of islet culture solution. The isolated islets were hand-picked with a pipette and counted. Finally the islets were placed in a humidified incubator at 37°C and 5% CO2 for *in vitro* GSIS. The islets were extracted with acidic ethanol overnight to obtain insulin content, which is then measured by ELISA. For inhibitor treatment, islets need to be incubated in culture solution with 1% DMSO or 10 μM fatostatin hydrobromide (HY-14452A, MCE, USA) for 24 h prior to subsequent experiments. The islets used for protein and total RNA extraction were collected in 1.5 ml Eppendorf tubes and centrifuged at 1500g for 3 minutes. After the supernatant was discarded, the islets were stored at -80°C and could also be used for TEM sample preparation.

Insulin and proinsulin measure using ELISA method

The insulin and proinsulin concentration from *in vivo* GSIS and lysed isolated islets was measured using Mouse INS and PI ELISA Kit (69-21071/69-21129, MSKBIO, China) and according to the kit instructions. The concentration data was normalized to the total DNA content.

RT-PCR analysis

Total RNA was extracted using the RNAiso Plus (9109, Takara, Japan) method according to the manufacturer's protocol and reverse transcribed into cDNA using a cDNA synthesis kit (AT311, TransGen Biotech, China). Real-time PCR was performed with a Tip Green qPCR SuperMix kit (AQ142, TransGen Biotech, China) and a LightCycler 96 Instrument (Roche Molecular Systems, USA). *GAPDH* was used as an internal standard. The relevant primer sequences for RT-PCR were listed in Table S1. The PCR reactions were 95°C for 2 min, and then 40 cycles of 95°C for 5 s, 58°C for 15 s, and 72°C for 34 s, followed by extension at 72°C for 5 min. Target gene mRNA level was normalized to that of *GAPDH* in the same sample using the $2^{-\Delta\Delta Ct}$ method. Each sample was measured in triplicate in each experiment. Moreover, melting curves for each PCR product were analyzed to ensure the specificity of the amplification product.

Protein extraction and Western blotting

Proteins were extracted using RIPA Lysis buffer (C5029, Bioss, China) supplemented with protease and phosphatase inhibitor cocktail (P1050, Beyotime, China) from frozen islets or tissues by ultrasonic crushing or grinding, respectively. Subsequently, protein concentration was measured by BCA Assay Kit (P0012, Beyotime, China). Equal amounts of proteins were loaded and separated by SDS-PAGE and transferred onto nitrocellulose membranes. The membranes were blocked at room temperature for 1 h in TBST buffer containing 5% skimmed milk or BSA. Immunoblotting was conducted with the indicated primary antibodies overnight at 4°C and horseradish peroxidase-conjugated secondary antibodies (Table S2) at room temperature for 1 h. After each antibody incubation, the membranes were washed for 8 min with TBST buffer for 3 times. Subsequently, the immunoreactive signals were detected using a Universal ECL Substrate (BMP3010, Abbkine, USA) and recorded with a ChemiDoc XRS+ (Bio-Rad, USA). The images were analyzed using NIH ImageJ software.

Immunohistochemistry

The pancreas tissues were fixed with 4% paraformaldehyde for at least 24 h. Paraffin embedded tissues were cut into 5 μm sections. Following deparaffinization with xylene, the sections were rehydrated with ethanol. An antigen retrieval buffer based on citrate was used (C1032, Solarbio, China) for heat-mediated antigen retrieval. Samples were incubated overnight at 4°C with proinsulin antibody (ab243141, Abcam, USA, 1:200) or CPE antibody (sc-393761, Santa Cruz Biotechnology, USA, 1:200). The staining signal was detected using SP link Detection kit (SP-9001, ZSGB-Bio, China) and DAB kit (ZLI-9017, ZSGB-Bio, China). For INS immunofluorescence, insulin rabbit mAb (A19066, Abclonal, USA) and fluorescent secondary antibody (A23420, Abbkine, USA) were used, and nuclei were stained with DAPI (P0131, Beyotime, China). The intensity of fluorescence signals and the average integrated optical density per area (IOD/Area) was measured by NIH ImageJ software.

TEM and images analysis

After fixation with 2.5 % glutaraldehyde solution overnight at 4°C, isolated islets were post-fixed with 2 % OsO_4 and stained in 2.5 % uranyl acetate. Digital images were acquired with JEM 2000EX (JEOL, Japan) and a Megaplus camera system operated with AMT software. The density and maturity rate of SGs in the images were quantified by NIH ImageJ software.

Luciferase reporter assays

HEK293T cells transfected with pcDNA3.1 or pcDNA3.1-SERBP1 plasmid, with pGL4.10, eIF4G1-WT or eIF4G1-MUT plasmid. Renilla luciferase was co-transfected for the purposes of normalization. Cells were harvested 24 hours after transfection and assayed for firefly luciferase and Renilla luciferase activities by Dual Luciferase Reporter Gene Assay Kit (KTA8010, Abbkine, USA).

QUANTIFICATION AND STATISTICAL ANALYSIS

Data are shown as mean ± SEMs. Statistical analysis was performed using a student's t test with GraphPad Prism 9.0 (www.graphpad.com). Statistical significance is considered at p values below 0.05. *$p < 0.05$; **$p < 0.01$, and ***$p < 0.001$. Statistical parameters including exact n and what n represents are reported in the Figures and Figure Legends. Blotting and IHC quantification were analyzed using NIH ImageJ software.